Received: 5 July 2018 | Accepted: 26 November 2018

DOI: 10.1002/dep2.55

ORIGINAL RESEARCH ARTICLE

WILEY The Depositional Record Open Access
The journal of the International Association of Seidmentologisits

# Banded Iron Travertines at the Ilia Hot Spring (Greece): An interplay of biotic and abiotic factors leading to a modern Banded Iron Formation analogue?

**Christos Kanellopoulos**[1,2] | **Camille Thomas**[2] | **Nikolaos Xirokostas**[3] | **Daniel Ariztegui**[2]

[1]Department of Geology and Geoenvironment, National and Kapodistrian University of Athens, Athens, Greece

[2]Department of Earth Sciences, University of Geneva, Geneva, Switzerland

[3]Institute of Geology and Mineral Exploration (I.G.M.E.), Acharnae, Greece

**Correspondence**
Daniel Ariztegui, Department of Earth Sciences, University of Geneva, Geneva, Switzerland.
Email: daniel.ariztegui@unige.ch

**Funding information**
Schweizerischer Nationalfonds zur Förderung der Wissenschaftlichen Forschung, Grant/Award Number: 200021_166308/1; This institution has not funded the research. We thank it for the support and collaboration in the acknowledgments

## Abstract

A hot spring at Ilia in the Greek Island of Euboea precipitates iron-rich travertine at an ore-grade concentration (up to 35.3 wt% Fe). This hydrothermal chemical sediment system deposits bands of iron oxyhydroxides (ferrihydrite), millimetres to centimetres thick, alternating with calcium carbonate-dominated layers, creating "Banded Iron Travertine" (BIT). The ferrihydrite laminae display a dendritic texture formed of spherical nodules often covering filaments identified as bacterial stalks of Zetaproteobacteria. These microaerophilic iron-oxidizing bacteria were identified by their 16S rRNA gene sequences in ferrihydrite-enriched samples from areas under high water flow. They were missing in the aragonite/calcite-dominated samples exhibiting features of aerial exposure and cyanobacteria instead. These characteristics, and the relative depletion in Fe-rich layers of redox-sensitive elements like Mn and Ce, as well as the presence of halite in Ca-rich layers, suggest that the bands form by successive changes in hydrothermal flow. This allowed microaerophilic iron oxidation to form Fe-rich layers, while Ca-rich bands precipitated when the hydrothermal water had time to equilibrate with the atmosphere. This sea water-dominated hydrothermal system is enriched in reduced iron and rapidly precipitating carbonates and ferrihydrite in the form of bands, having similarities to "Banded Iron Formation" (BIF). BIF represents archives of Earth's primitive biogeochemistry although the combined abiotic and biotic processes that have likely led to their formation are not fully resolved. Diagenesis and metamorphism have a strong imprint on BIF. Thus, continuous efforts are pursued to identify modern analogues that could help unravel their formation. Although carbonate is not a common feature of BIFs, Ilia system provides an interesting analogue for their depositional processes and potential microbial–mineral associations they may have hosted. It also presents pre-diagenesis facies association and mineralogy that could bring new clues for unravelling BIF modes of formation and the salient biogeochemical conditions characteristic of their original depositional environment.

**KEYWORDS**
calcium carbonates, ferrihydrite, hydrothermal springs iron-rich thermogenic travertines, *Zetaproteobacteria*

## 1 | INTRODUCTION

Among the most important iron ore deposits on Earth are the spectacular and enigmatic Banded Iron Formations (BIFs). Despite extensive studies, their modes of depositions have not been fully resolved; although one of the prevalent models is that BIFs are thought to be the result of the reaction between hydrothermal reduced iron, and photosynthetically produced oxygen. Microbes are generally recognized as important contributors to the specific sedimentological conditions of these deposits, both regarding the processes of primary iron oxidation and secondary iron reduction (Posth, Konhauser, & Kappler, 2013). Since BIFs likely hold information on some of the earliest forms of life on Earth, they are extensively investigated and analogues for their mode of formation are thoroughly searched for.

Active hydrothermal iron-rich deposits are among the targets of this search. They can be found in terrestrial environments, that is, iron-rich thermogenic travertines (Kanellopoulos, Mitropoulos, Valsami-Jones, & Voudouris, 2017; Takashima & Kano, 2005; Takashima, Okumura, Nishida, Koike, & Kano, 2011) and in submarine hydrothermal environments (Bortoluzzi et al., 2017; Kilias et al., 2013; Pichler & Veizer, 1999). In these systems, the presence of microbial activity is most often identified at redox interfaces and has been suggested to play an active role in the formation of iron minerals such as iron oxides (Kappler & Newman, 2004; Konhauser, 1998; Widdel et al., 1993). Hot springs are ideal environments for iron oxidation, since the hydrothermal fluid is often enriched in Fe(II) and free of oxygen. In such conditions, a steep redox gradient develops in the water immediately adjacent to the spring vent through uptake of atmospheric $O_2$ (Takashima, Kano, Naganuma, & Tazaki, 2008). In near neutral pH hydrothermal springs, the Fe-rich deposits consist primarily of ferric hydroxides (commonly as ferrihydrite). These ferric hydroxides precipitate readily abiotically in oxygenated environments or their precipitation can be microbially mediated and influenced (Chan, Fakra, Emerson, Fleming, & Edwards, 2011; Konhauser, 1998). When microbes are involved, rates of iron mineralization can increase four-fold (Kasama & Murakami, 2001). These processes generally occur at redox interfaces, where iron-oxidizing bacteria are commonly found and where microaerophilic conditions dominate (Konhauser, 1998). Such conditions have been suggested in the formation of BIFs, and iron-oxidizing bacteria as associated with the formation of iron bands in Precambrian BIFs (Chaudhuri, Lack, & Coates, 2001; Holm, 1987; Konhauser et al., 2002). However, the study of iron mineralization in hydrothermal systems is often hampered by the poor accessibility of active sites, and the instable characteristics of ferrihydrite therein.

This study characterizes the iron-rich thermogenic travertines of Ilia, on the Greek island of Euboea. The depositional system hosts almost pure ferrihydrite lamina which, together with fast precipitation rates, high iron enrichment and specific hydrothermal chemistry (Kanellopoulos et al., 2017) provides a unique setting for the study of laminated iron chemical sediments. The purpose of the work presented in this paper is to understand the depositional processes leading to the formation of laminated iron-rich deposits in Ilia and to further link them to BIF depositional models. This study documents the geochemistry of the Fe-rich hydrothermal fluids from the Ilia area, the macrofacies and microfacies, the petrographical characteristics, mineralogical and geochemical composition of the newly formed iron-rich thermogenic travertine, and the microbial communities associated with the different facies of this deposit. The Fe-rich travertine is compared with active hydrothermal systems elsewhere and all of the available data synthesized to propose a model for Banded Iron Travertine (BIT) deposition, with possible analogy to the formation of BIFs. The goal is to provide a depositional model associated to an easily accessible and dynamic system precipitating banded iron-rich chemical sediments.

## 2 | GEOLOGICAL SETTING

Ilia is located in the north-western part of Euboea Island, Greece (Figure 1). The geological setting of the region is unique since it is located at the western extremity of the North Anatolian Fault and is in a back-arc position with respect to the South Aegean Active Volcanic Arc (Pe-Piper & Piper, 2002; Ring, Glodny, Will, & Thomson, 2010; Vött, 2007). It is one of the most neo-tectonically active areas in Greece dominated by extensional tectonics similarly to the rest of the Aegean Sea.

Ilia's hot spring, that is, artesian borehole (38° 51′ 07″ N, 23° 07′ 44″E) is one surface manifestation of a large geothermal system with other surface manifestations of hot springs in northern Euboea island and the neighbouring area of Sperchios (mainland; Kanellopoulos, 2011; Kanellopoulos et al., 2017). This hydrothermal system is controlled by active tectonics and supplied with heat by a deep magma chamber (Kanellopoulos et al., 2017), identified at depths of 7–8 km under the Northern Euboean Gulf (Karastathis et al., 2011), which has the Plio-Pleistocene trachyandesitic volcanic centre of Lichades as a surface manifestation. A salient feature of Euboea's hot springs is the dominance of thermogenic travertine deposition (Kanellopoulos, 2011, 2012, 2013) including the Fe±As -rich ore-bearing travertines of Ilia (Kanellopoulos, 2011, 2012; Kanellopoulos et al., 2017).

The hydrothermal fluids of northern Euboea's hot springs have near neutral pH and a sodium-chloride composition. They are similar in their chemical characteristics

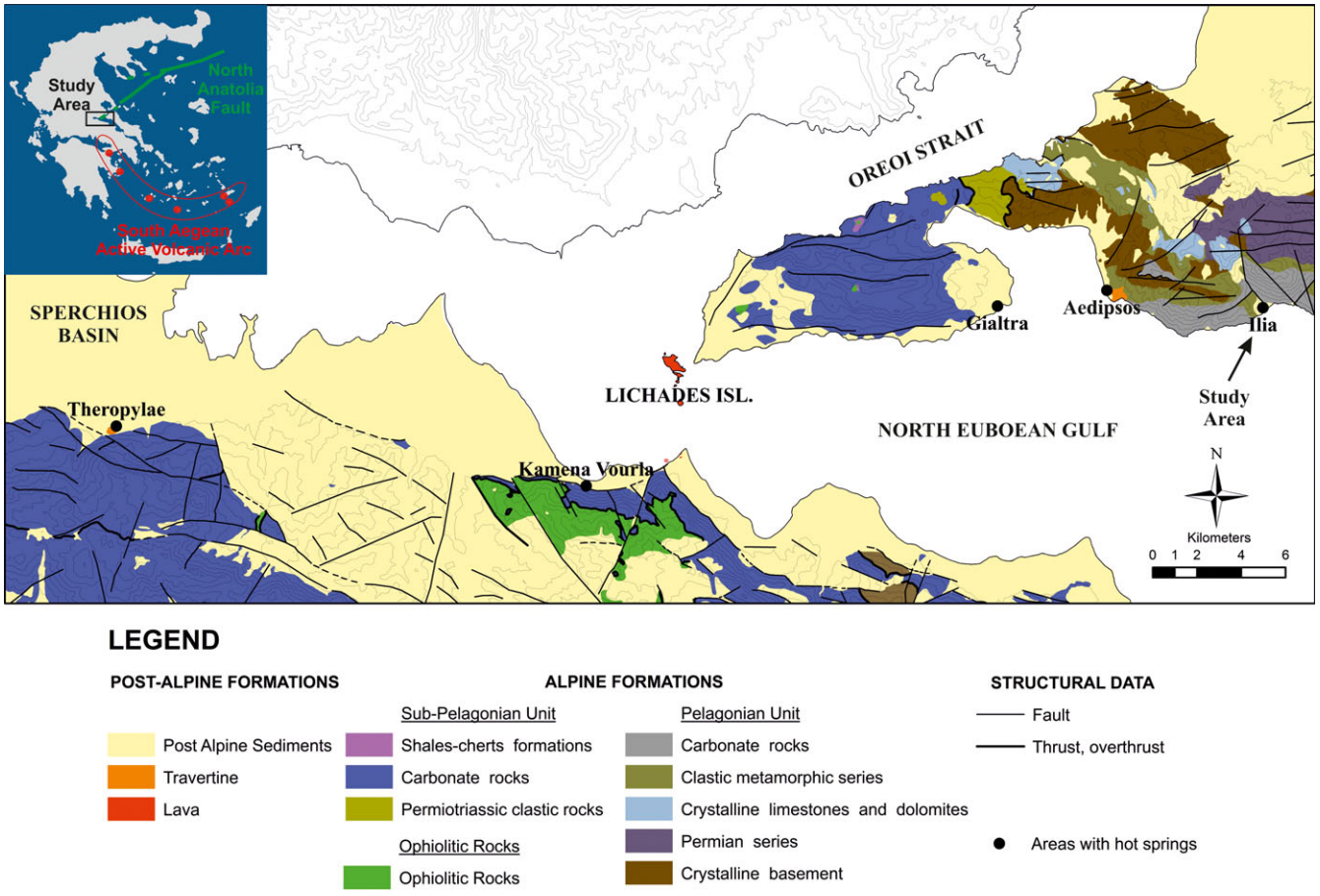


**FIGURE 1** Simplified geological Map of Northern Euboea Island, Greece (after Kanellopoulos et al., 2018)

and are classified as deep geothermal fluids, with volcanic origin affinities (Kanellopoulos et al., 2017). Based on geochemical and isotopic studies (Dotsika, 2015; Kanellopoulos, 2011; Kanellopoulos et al., 2017; Shimizu, Sumino, Nagao, Notsu, & Mitropoulos, 2005), their chemistry is controlled mainly by contribution of three components: (a) high sea water participation, (b) deeper magmatic fluids, and (c) the local bedrock. The chemical composition of the thermogenic travertine, together with drilling data (Gkioni-Stavropoulou, 1998; Hatzis, Kavouridis, Bakalopoulos, & Xenakis, 2008; Kanellopoulos et al., 2017), strongly suggests that the source of calcium for the extensive travertine deposits of Euboea is the dissolution by geothermal fluids of marble/limestone located below the metamorphic sequence of Aedipsos and Ilia.

## 3 | MATERIAL AND METHODS

### 3.1 | Hot water samples

Hydrothermal fluid samples from the hot spring/artesian borehole were collected from the mouth of the pipe (Figure 2a–d). Physicochemical parameters such as temperature, pH, electrical conductivity (E.C.), and total dissolved solids (T.D.S.) were measured in situ, using portable probes. The pH-meter was calibrated with standard buffer solutions of pH 4.0 and 7.0 before any measurements were taken. The pH measurement error, including accuracy and reproducibility, is better than ±0.05 pH units. Temperature was measured with the probe connected to the pH-meter and the error is estimated to be less than ±0.3°C. Moreover, a thermal imaging camera was used in order to present through thermal images the temperature changes at the sampling site. Thermal imaging camera is a type of thermographic camera, which is reading infrared radiation as visible light and allows us to see areas of heat through water or solid rock.

Water was collected in polyethylene bottles for laboratory analyses. Aliquots of 250 ml intended for the determination of trace elements were acidified to pH < 2 with analytical grade $HNO_3$ (Suprapur 65%). All samples were stored in a portable cooler containing ice packs, transported to the laboratory and refrigerated at 4°C until analysis. One-litre aliquots (non-acidified) were filtered in the laboratory before major ion determinations.

The major ion concentrations were measured using spectrophotometry, titration, and Inductively Coupled Plasma-Optical Emission Spectrometry (ICP-OES; Perkin


**FIGURE 2** Paired views of Ilia's hot spring pictures and corresponding thermal images of the same area. In the right side of each thermal picture, a colour column shows the temperature scale corresponding to the colours. (a and b) General view of the hot water venting out from the pipe. (c and d) Close view of the pipe end point. (e) Venting point of the hot water and associated deposition. Orange-yellowish colour component is Ca-rich and brownish-metallic colour component is Fe-rich. At close-up image (f) could be observed that inside the Ca-rich component are developing Fe-rich bands (see red arrows)

Elmer Optima 5300 DV). The trace element concentrations were measured using Inductively Coupled Plasma-Mass Spectrometry (ICP-MS; Perkin Elmer Sciex Elan 6100).

## 3.2 | Travertine samples

The hydrothermal spring of Ilia vents from an artesian borehole accessible from the road that run along the beach. The water then flows along a 3–5 m long pipe and out onto the beach (Figure 2). Samples of thermogenic travertine were collected from the top part of the borehole, from the venting point of the pipe and from the deposits at the beach (Figure 2). The mineralogical composition of the main mineral phases in these travertines was identified with X-Ray Diffraction (XRD) using a Siemens Model 5005 X-ray diffractometer, Cu Ka radiation at 40 kV, 40 nA, 0.020° step size, and 1.0 sec step time. The XRD patterns were evaluated using the EVA program of the Siemens DIFFRACplus and the D5005 software package. The minor mineral phases were identified by Scanning Electron Microscopy (SEM) and Energy Dispersive Spectroscopy (EDS). The SEM-EDS analyses were carried out using a Jeol JSM 5600 SEM instrument, equipped with an Oxford ISIS 300 micro analytical device.

The travertine samples were analysed for whole rock geochemistry after drying and pulverizing in an agate mortar and mill to less than 0.075 mm. The samples were digested with a mixture of HCl-$HNO_3$-HF acids and analysed with Inductively Coupled Plasma–Optical Emission Spectroscopy method (ICP-OES; Perkin Elmer Optima 5300 DV) for Ca, Na, P, S, Si, and by Inductively Coupled Plasma-Mass Spectrometry method (ICP-MS; Perkin Elmer Sciex Elan 6100) for a series of trace elements, including rare earth elements (REE). Analytical data quality was tested with internal standards, certified and in-house reference materials in random positions within the analytical batch and by blank analysis and duplicate analysis of a proportion of the samples (Ramsey, Thompson, & Banerjee, 1987).

## 3.3 | Molecular biology

Samples for microbiological studies were collected at the vent of the artesian borehole (Ilia Drill for ID-labelled

samples, Figure 3a,b) and at the pipe outlet (Ilia Pipe for IP-labelled samples, Figure 3c,d). They experienced different environmental conditions at time of sampling, which are detailed in Table 1.

Hard rock samples were taken using a chisel and a hammer cleaned and sterilized with ethanol. Soft material was sampled using a sterile scalpel. All samples were stored in 50 mL falcon tubes or zip-lock bags and kept at −20°C until further processing. Hard rock samples were then crushed under clean conditions in a sterilized agate mortar. Two grams of processed sample was used for DNA extraction using the MOBIO power soil kit. Triplicate DNA amplification was realized with a total of ~10 ng of DNA per triplicate using universal primer 515F (5′-GTGYCAGCMGCCGCGGTA-3′) and 909R (5′-CCCCGYCAATTCMTTTRAGT-3′) for the V4-V5 hypervariable region of the 16S rRNA gene (Wang & Qian, 2009), with indexes integrated following the dual-indexing procedure described by Kozich, Westcott, Baxter, Highlander, and Schloss (2013). Product triplicates were then pooled, quantified using Picogreen assay (Life Technologies) and pooled equimolarly. The final pool was concentrated using a SpeedVac Plus SC110A Savant and purified with CleanNA beads (Moka science).

Sequencing was performed by Fasteris (Geneva, Switzerland) on an Illumina Miseq with 2 × 250 cycles, with settings of 7.5 Gb yield (including PhiX), an error rate of 2.5% and Q30 at 75%. The analysis yielded 5.3 Gb of sequences with an error rate within quality specifications. Adapters were removed using trimmomatic (Bolger, Lohse, & Usadel, 2014), paired-ends reads were joined using ea-utils (Aronesty, 2011), quality checks were performed using FastQC, and samples were demultiplexed using the Fasteris in-house script. Fasteris also did all the downstream work described above.

DNA-derived 16S rRNA gene sequences were processed using Mothur (Schloss et al., 2009). Samples were dereplicated, aligned, and filtered by length. Chimeras were removed using uchime (Edgar, Haas, Clemente, Quince, & Knight, 2011), and taxonomic affiliation was then realized using the method of Wang, Garrity, Tiedje, and Cole (2007) at a cutoff of 80% against the Silva SSU database 123 (Quast et al., 2013). Operational Taxonomic Units (OTU) were then defined at a 97% similarity and used for similarity analysis. Random subsampling was realized based on the smallest number of obtained sequences in one sample after singleton removal (see Tables S1 and S2 for more details). A matrix was built at the phylum level (excluding phyla that accounted for less than 1% of the total community) and Principal Component Analysis (PCA) was performed using Past (Hammer, Harper, & Ryan, 2001). Sequences were submitted to NCBI and can be found under the accession number MH385389 – MH388018.

## 4 | RESULTS

### 4.1 | Water chemistry

Based on repeated measurements conducted over the sampling period and the previous years (Kanellopoulos et al., 2017), the physicochemical parameters of the hydrothermal fluid have only limited variation, with temperature varying from 60.9 to 63.7°C and acidic pH values varying from 5.88 to 6.45 (Table 2, Figure 2).

Table 2 shows the physicochemical and chemical parameters analysed in situ and in the laboratory. Chloride is the dominant anion of the Ilia fluid (1.28% Cl). Based

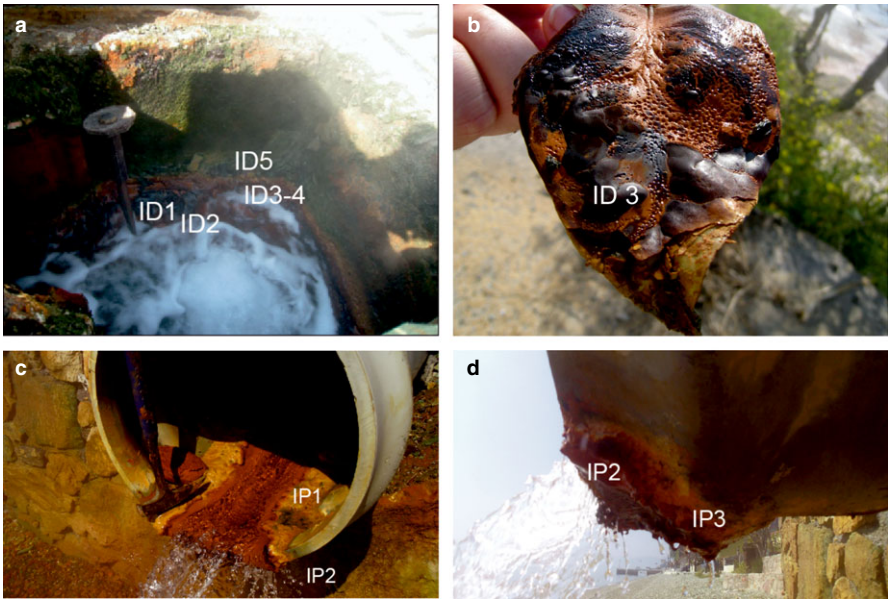


**FIGURE 3** Position of the different samples used for microbiological study. (a) Artesian borehole and locations of the ID samples. (b) Ferrihydrite encrusted leaf, from the borehole. (c) Pipe outflow where IP samples were taken. (d) Localization of IP2 and IP3 underneath the pipe opening

**TABLE 1** Microbiological sample description and characteristics

| | Site | Water flow | Light exposure | Air exposure | Composition | Commentaire |
|---|---|---|---|---|---|---|
| ID1 | Borehole | No | No | Buried | Black mat | Black unconsolidated material, EPS like |
| ID2 | Borehole | High | No | No | Ferrihydrite crust | Black crust |
| ID3 | Borehole | Moderate | Moderate | No | Ferrihydrite crust | Black crust on leaf |
| ID4 | Borehole | No | No | Buried | Black crust | Underneath black crust |
| ID5 | Borehole | Low | Yes | Yes | Mixed mat | Black crust cyano mat in contact with black |
| IP1 | Pipe mouth | Low | Yes | Yes | $CaCO_3$ crust | Cyano mat in pipe |
| IP2 | Pipe mouth | High | Moderate | No | Mixed crust | Below pipe |
| IP3 | Pipe mouth | Moderate | Moderate | No | Mixed crust | Below pipe off light little flow |

on the hydrochemical analyses (Table 2), the fluid is characterized by Na-Cl hydrochemical type. Specific enrichment exists in major elements such as Fe (13.3 mg/L) and Ca (1,570 mg/L) and in trace elements such as As (up to 250 μg/L), Mn (500 μg/L), Ni (up to 80 μg/L), and ammonium cation (up to 1.9 mg/L $NH_4^+$, Table 2). It also shows concentrations of Sr of 24 mg/L, B of 9.7 mg/L, F of 3.8 mg/L, and Li of 3.4 mg/L.

## 4.2 | Morphology of the travertine deposit

Ilia's hot water artesian borehole deposits thermogenic travertine at the discharge point, along the pipe, at the mouth of the pipe and at its outflow on the beach, building up the sides of a keel that slowly rises in height with time (Figures 2 and 3). Precipitation also occurs below the pipe as the water flows on the wall and onto the beach (Figures 2e,f and 3d) although deposition practically stops only a few metres from the pipe. Travertine deposition is also taking place inside the borehole (Figure 3a). Periodic intervention of the local authorities to remove the deposits prevents the borehole and pipes from becoming completely clogged.

The thermogenic travertine (Figure 4) at the discharge point consists of separate Fe-rich (brownish-metallic colour) and Ca-rich (orange-yellowish colour) laminae/bands up to a few centimetres thick (Figure 4b–d). The travertine macrofacies consists of laminated specular, knob-like, and botryoid shapes (Figure 4) which evolve into a dense layered crystalline travertine crust at the pipe mouth (Figures 2a,b,e,f and 4a,b) forming bands (Figure 4c,d,f) or thin layers (Figure 4e,f) usually botryoidal in shape. A vertical cross-section through several samples revealed a well-developed laminated texture in all of them (Figure 4c–f), with band thickness ranging from submillimetre (Figure 4f) to centimetre scale (Figure 4c,d).

Based on field observations, Ilia deposition is mainly orange in colour, suggesting Ca-rich component dominates. This colour expands along the hot water flow, until it reaches the sea. Dark-brown to black-coloured surfaces (Fe-rich component) are observed where the hot water with a high flow rate reaches the ground; in the top part of the borehole where water level changes due to degassing (Figure 3a); and inside the pipe, especially at water level, which changes depending on the water flow (Figure 2c–f).

## 4.3 | Mineralogical study and microfacies of the travertine deposit

Samples from Fe-rich and Ca-rich components were separated and analysed by XRD (Figure 5a). Based on these analyses, the Fe-rich component is composed mainly of two-line ferrihydrite and to a lesser extent of aragonite and calcite (Figure 5b), as previously described by Kanellopoulos (2012) and Kanellopoulos et al. (2017). The Ca-rich component is composed mainly of aragonite and calcite with a minor contribution from ferrihydrite and halite (Figure 5c).

Under the optical microscope, the Fe-rich and Ca-rich bands are markedly distinct (Figure 6a). The Ca-rich bands are mainly laminated (Figure 6b), consisting of needle-like crystals of aragonite, growing normal to the substrate (Figure 6c). The crystals are elongated parallel to the c-axis, exhibiting straight extinction. The substrate is usually a thin lamina of silt-sized micritic aggregates (Figure 6c) or another Fe-rich lamina. In several cases, parallelogram-shaped areas of aragonite, with rounded edges, are observed developing within Fe-rich masses (Figure 6d), suggesting the complex 3-D spatial spreading of the two main components (i.e., Fe-rich and Ca-rich components).

Under the optical microscope, the Fe-rich components mainly consist of dark red to brown ferrihydrite. Combined optical microscope observations and SEM images show two ferrihydrite facies. The first type consists of laterally aligned shrub-like structures extending and branching upwards and forming laminae (Figures 6e–g and 7a,b).

**TABLE 2** Physiochemical parameters, major ions, and trace elements concentrations from the studied hot spring and others terrestrial hot springs and hydrothermal submarine vents depositing ferrihydrite

| | Terrestrial | | | | Submarine | | | Sea water |
|---|---|---|---|---|---|---|---|---|
| | Ilia, Euboea-Greece*[1] | Ilia, Euboea-Greece*[1] | Shionaha-Japan*[2] | Okuoku-hachikurou-Japan*[3] | Basiluzzo Islet-Italy*[4] | Kolumbo-Greece*[5] | Tutum Bay-Papua New Guinea*[6] | SW, Aegean Sea-Greece*[7] |
| T (°C) | 63.5 | 63.7 | 37.8 | 43.3 | – | – | – | 25.9 |
| pH | 5.9 | 6.1 | 6.38 | 6.6 | 5.7 | 5 | 6.1 | 8.18 |
| E.C. (mS/cm) | 34,150 | 34,400 | – | – | 33,300 | – | – | 56,350 |
| T.D.S. (mg/L) | 23,200 | 22,700 | – | – | – | – | – | 40,900 |
| $Ca^{2+}$ (mg/L) | 1,420 | 1,570 | 350 | 790 | 2,770 | – | 201 | 475 |
| $Mg^{2+}$ (mg/L) | 190 | 230 | 34.2 | 150 | 3,690 | – | bdl | 1,160 |
| $Na^{+}$ (mg/L) | 6,940 | 6,760 | 534 | 510 | 21,780 | – | 650 | 13,240 |
| $K^{+}$ (mg/L) | 180 | 210 | 90 | 25 | 1,790 | – | 76 | 423 |
| $HCO_3^{-}$ (mg/L) | 640 | 640 | – | – | – | – | 840 | 168 |
| $Cl^{-}$ (mg/L) | 12,550 | 12,800 | 712 | 1,270 | 31,530 | – | 295 | 22,270 |
| $SO_4^{2-}$ (mg/L) | 810 | 800 | | 770 | 660 | – | 930 | 3,257 |
| $NO_3^{-}$ (mg/L) | bdl | bdl | – | bdl | – | – | – | <5 |
| $NH_4^{+}$ (mg/L) | 1.9 | 0.6 | – | – | – | – | – | <0.05 |
| $NO_2^{-}$ (mg/L) | bdl | bdl | – | – | – | – | – | <0.05 |
| $F^{-}$ (mg/L) | 3.6 | 3.8 | – | – | – | – | – | 2.45 |
| $SiO_2^{-}$ (mg/L) | 100 | 50 | 82.1 | 51,279.021 | 53,696.43 | – | 231 | 5 |
| Ag (μg/L) | bdl | bdl | – | – | | 191,000 | – | – |
| Al (μg/L) | bdl | bdl | – | – | 320,000 | 3,240,000 | – | 105 |
| As (μg/L) | 250 | 150 | – | – | 520,000 | 0.29 (%) | 820 | <10 |
| B (μg/L) | 9,700 | 9,200 | – | – | – | – | 8,400 | 13,800 |
| Ba (μg/L) | 190 | 210 | – | – | – | – | – | <10 |
| Be (μg/L) | bdl | bdl | – | – | – | – | – | – |
| Br (μg/L) | 40,300 | 38,100 | – | – | 100,000 | – | 6,800 | 87,300 |
| Cd (μg/L) | bdl | bdl | – | – | – | – | – | – |
| Co (μg/L) | bdl | bdl | – | – | – | – | – | – |
| Cr (μg/L) | bdl | bdl | – | – | 0.1 (%) | – | – | – |
| Cu (μg/L) | 70 | 130 | – | – | 23,500 | 1,510 | – | 120 |
| Fe (μg/L) | 11,300 | 13,300 | 12,100 | 6,800 | 314,500 | 24.2 (%) | 1,720 | 52 |
| Hg (μg/L) | bdl | bdl | – | – | – | 0.1 (%) | – | – |
| I (μg/L) | 560 | 500 | – | – | – | – | – | – |
| Li (μg/L) | 1,900 | 3,360 | – | – | – | – | 1,020 | 3,360 |
| Mn (μg/L) | 380 | 500 | – | – | 170,000 | – | 495 | <10 |
| Mo (μg/L) | bdl | bdl | – | – | 173,000 | – | – | 30 |
| Ni (μg/L) | 75 | 80 | – | – | 20,000 | 2.88 (%) | – | – |
| Pb (μg/L) | bdl | 20 | – | – | 39,000 | – | – | – |
| Rb (μg/L) | 220 | 190 | – | – | – | | 350 | – |
| Sb (μg/L) | bdl | bdl | – | – | – | 0.57 (%) | 8.2 | – |
| Se (μg/L) | 310 | 220 | – | – | – | – | – | – |
| Sr (μg/L) | 18,000 | 24,000 | – | – | – | – | 6,790 | 5,800 |

*(Continues)*

**TABLE 2** (Continued)

| | Terrestrial | | | | Submarine | | | Sea water |
|---|---|---|---|---|---|---|---|---|
| | Ilia, Euboea-Greece*[1] | Ilia, Euboea-Greece*[1] | Shionaha-Japan*[2] | Okuoku-hachikurou-Japan*[3] | Basiluzzo Islet-Italy*[4] | Kolumbo-Greece*[5] | Tutum Bay-Papua New Guinea*[6] | SW, Aegean Sea-Greece*[7] |
| U (μg/L) | bdl | bdl | – | – | – | – | – | – |
| V (μg/L) | 80 | 70 | – | – | 408,000 | – | – | – |
| Zn (μg/L) | bdl | bdl | – | – | 30,000 | 0.26 (%) | – | <30 |

*Notes*. *1 = Vakalopoulos et al. (2016); *2 = Takashima and Kano (2005); *3 = Takashima et al. (2008); *4 = Bortoluzzi et al. (2017) (DFS1); *5 = Kilias et al. (2013) (NA014-027 Champagne active mound-2); *6 = Pichler and Veizer (2004) (Vents 1–3); *7 = Athanasoulis et al. (2016) (sea water analyses from Aegean Sea).

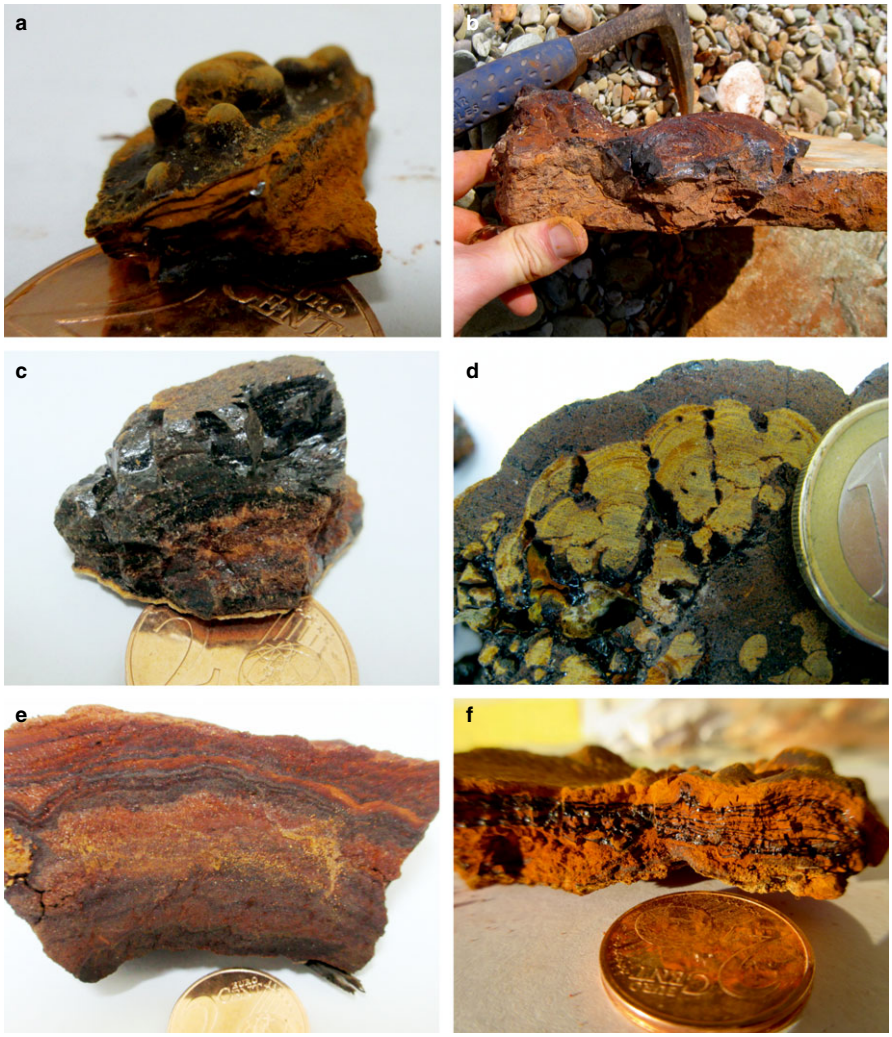


**FIGURE 4** Different macro- and microfacies of Ila Fe-rich travertine deposit. (a) Spicular, knob-like Fe-rich thermogenic travertine deposition from inside the borehole (upper part). (b) Dense Fe-rich travertine deposition. (e–f) Fe-rich laminae/bands with varying thickness from few mm up to few cm, alternating with Ca-rich laminae/bands

Typically, they are elongated, dense masses consisting of ferrihydrite micritic clumps, usually with spherical nodules creating "branches" and dendritic fabric (Figures 6e,f and 7f–h). Based on the classification scheme of Chafetz and Guidry (1999), they could be characterized as woody shrub or bush (i.e., bacterial shrubs). These shrubs are usually developed above aragonitic laminae (Figure 6e). In some cases, dark-tinted axes (filament-like), potentially consisting of organic matter, can be observed encased within the ferrihydrite shrubs (Figure 6g). The filaments extend and branch upwards, over a distance corresponding to the thickness of the lamina. Revealed under SEM, the iron-rich components of the studied samples are commonly composed of fine-scale laminae of the iron-rich mineral phase (ferrihydrite) alternating with calcium-rich (aragonite) laminae over a few tens of micrometres (Figure 7a).

Ferrihydrite has been observed in several cases to fill empty space between ferrihydrite shrubs, or between aragonite crystals (Figure 7e) creating very dense laminae. However, in several cases empty spaces between the dendrite aggregate were observed inside the laminae (Figure 7b).

Additionally, ferrihydrite was identified in a second type of facies consisting of dense laminae, with very limited porosity (Figures 6d,h and 7c–e). In this case, no crystalline habit or microfacies of the ferrihydrite could be identified. Although, the ferrihydrite laminae followed the geometry dictated by the substrate (i.e., Ca-rich laminae or bedrock).

Minor amounts of sulphides such as pyrite, As-rich pyrite, arsenopyrite, stibnite, galena, Fe-rich sphalerite, chalcopyrite and oxides, and non-metallic mineral phases such as barite, fluorite, and some REE-bearing phases, can be found in the studied samples. All of these minerals occur as very small crystals (few μm in size), in accordance to Kanellopoulos et al. (2017).

### 4.4 | Travertine geochemistry

Samples from Fe-rich and Ca-rich components were separated to analyse their bulk geochemical composition (Table 3). The Fe-rich component of the Ilia travertine is enriched compared to the Ca-component (and typical travertines) in Fe (35.3%), As (2.6%), and Na (4%) for major elements and in Y (323 mg/kg), Nd (96 mg/kg), Dy (63 mg/kg) for trace and rare earth elements (REE). In contrast, the Ca-rich components of the Ilia travertine are less enriched in all of these elements (11% Fe, 931 mg/kg As, 0.08% Na, inc. all the REE), but have higher concentrations of certain elements like Mn (330 mg/kg), S (0.27%), and other metals such as Co (0.24%), Cr (2.68%), and Ni (1.58%). Both components are presenting comparable concentrations to elements such as Cu (Fe-rich component: 6 mg/kg and Ca-rich component: 8.4 mg/kg), Mg (Fe-rich component: 1,915 mg/kg and Ca-rich component: 1,650 mg/kg), Pb (Fe-rich component: 4.7 mg/kg and Ca-rich component: 2.9 mg/kg), U (Fe-rich component: 240 μg/kg and Ca-rich component: 290 μg/kg), Zn (Fe-rich component: 63 mg/kg and Ca-rich component: 48 mg/kg).

Normalization of the whole rock chemical data to the average composition of Upper Continental Crust (UCC, Rudnick & Gao, 2003) and Post-Archaean Australian Shale (PAAS, Taylor & McLennan, 1985; Figure 8) indicates that both laminae are enriched in elements such as As, Fe, and S. The Fe-rich component in particular is enriched 5,440 times in As, compared to UCC abundances and almost 10 times in Fe, compared to UCC and PAAS abundances. Additionally, the Fe-rich component shows a clear enrichment in REE compared to UCC and PAAS, by more than 10 times (Figure 8). The two studied components show similarities with respect to light REE depletion, but the Ca-rich component has small positive anomalies in Ce and Y, which are not present in the Fe-rich component.

### 4.5 | Analysis of microbial communities based on 16S rRNA gene sequences

Microbial communities differ from each other based on sample lithology and exposure to water/air (Figure 9a). Bacteria-associated reads are dominant in all samples, but samples ID1 and ID4 have 19% and 26% of archaeal reads respectively, and IP2 and IP3 reach 44% and 28% (Figure 9a).

Principal component analysis shows the relationship between samples and the main phyla that characterize their relative composition (Figure 9b). Samples IP2 and ID2 are marked by a high number of *Aquificae* of the *Hydrogenotherma* genus (40% and 65%, respectively). They also share *Zetaproteobacteria* of the *Mariprofundales* genus with IP3 and ID3 (11% for IP2, 5% for ID2, 3% for ID3, and 7% for IP3). IP3 and ID3, together with IP1 and ID5, are clearly characterized by *Alphaproteobacteria* and *Cyanobacteria*. *Alphaproteobacteria* are generally represented by unclassified members as well as *Rhodobacterales, Rhodospiralles, Erythrobarcteraceae,* and *Rhizobiales*. ID1 and ID4 are both characterized by a large number of *Thaumarchaeota* (15% and 10%, respectively), *Planctomycetes* (34% and 17%, respectively), *Chloroflexi* (28% and 26%), *Deltaproteobacteria* (9% and 10%), and finally *Deferribacteres* (5% and 8%). *Nitrospira* are found in ID4, ID3 (13%) and form a significant portion of the *Thermodesulfovibrio*-associated sequences. Sample ID2, however, is dominated by unclassified *Nitrospira* sequences (11% of the total relative abundance).

Clades involved in iron reduction and oxidation are abundantly represented in the samples of the Ilia travertine. Members of the iron-oxidizing *Zetaproteobacteria* represent 3% of the community in ID2 and ID3. This clade is even more abundant in the Ilia pipe samples, where they correspond to 10% and 7% of IP2 and IP3 microbial communities, respectively. The presence of unclassified *Rhodobacteracea* may also be related to phototrophic iron oxidation, but this is not certain.

## 5 | DISCUSSION

### 5.1 | Hydrothermal fluid

The hot spring/artesian borehole of Ilia degases mainly $CO_2$ (D'Alessandro, Brusca, Kyriakopoulos, Bellomo, & Calabrese, 2014) and deposits Fe±As -rich thermogenic travertine (Kanellopoulos, 2011, 2012; Kanellopoulos et al., 2017). It is part of a large single hydrothermal system,

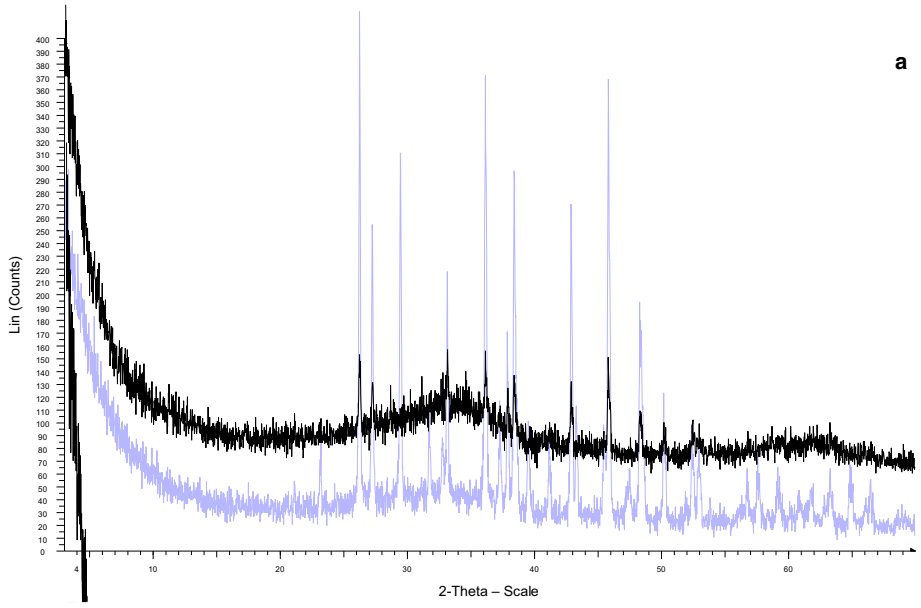
a
Lin (Counts)
2-Theta – Scale

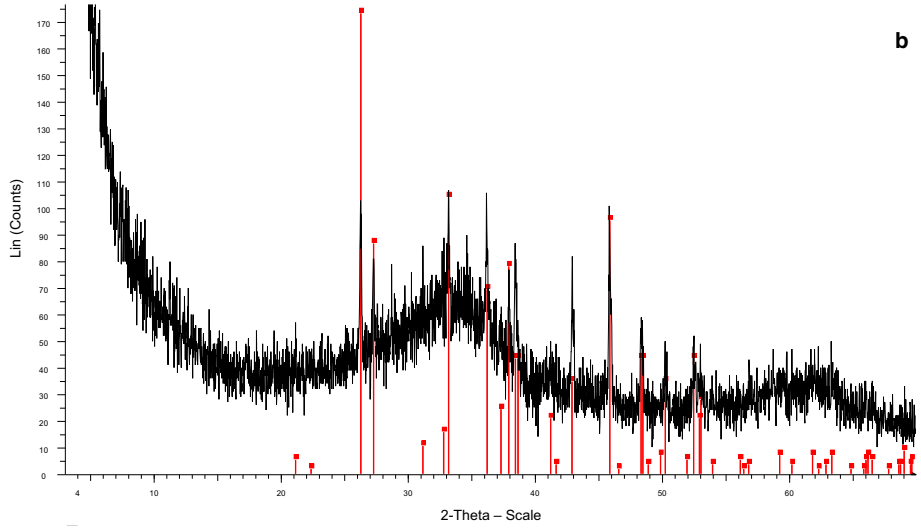
b
Lin (Counts)
2-Theta – Scale

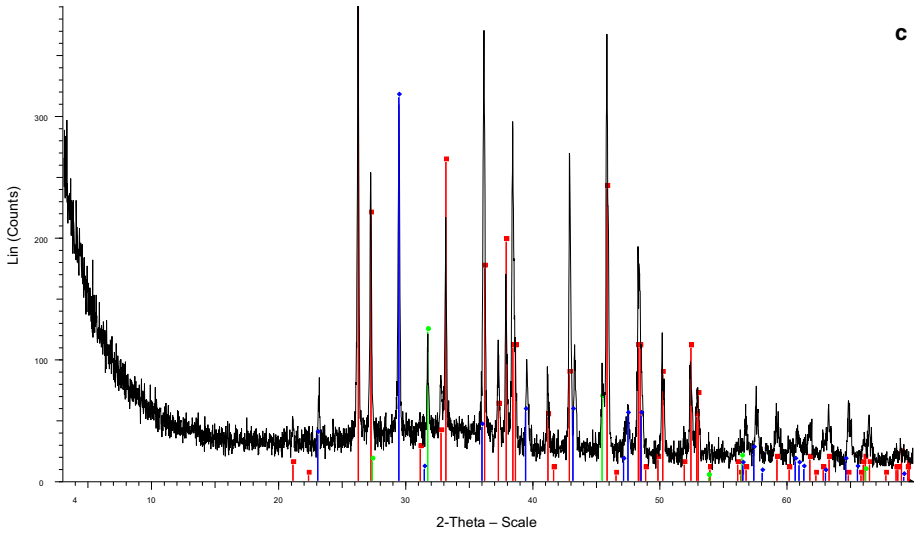
c
Lin (Counts)
2-Theta – Scale

**FIGURE 5** XRD pattern of Fe-travertine from Ilia. (a) Combined XRD patterns of selected material from pure Fe-rich (with black colour) and Ca-rich (with blue colour) bands. It is distinct the presence of the two characteristic broad peaks at around 35° and 62° in 2θ, which are typical of poorly crystalline two-line ferrihydrite and the sharp peaks corresponding to the other mineral phases. (b) XRD pattern of selected material from pure Fe-rich bands (red colour = aragonite). (c) XRD pattern of selected material from pure Ca-rich bands (red colour = aragonite, blue colour = calcite, green colour = halite)

which occurs at the north-western part of Euboea island, and at the neighbouring area of mainland, that is, Sperchios area (Kanellopoulos et al., 2017; Figure 1). The hydrothermal fluids of NW Euboea's hot springs are near neutral pH, sodium-chloride, with very close chemical relation between them (Kanellopoulos et al., 2017). Ilia's hydrochemical fluid type is Na-Cl (Table 2), with chloride concentrations (i.e., 1.28% Cl) comparable to Aegean Sea sea water (2.2% Cl, Athanasoulis et al., 2016). However, Ilia's hydrothermal fluid has higher concentration of Sr (24 mg/L) and similar concentration of Li (3.4 mg/L) comparable to Aegean Sea sea water (5.8 mg/L for Sr; and 3.4 mg/L for Li; Athanasoulis et al., 2016). The Ilia hot spring/artesian borehole is located only few metres from the seashore. The dominant anion and cation in Ilia's hydrothermal fluid are chloride (up to 1.28%) and sodium (up to 0.7%). Additionally, the fluid shows high concentrations of a series of ions and trace elements (conservative constituents), typically associated with sea water or/and are likely to be of deep geothermal origin such as F, $SiO_2$, and Li. In accordance with the findings of previous studies (D'Alessandro et al., 2014; Dotsika, 2015; Kanellopoulos et al., 2017; Vakalopoulos et al., 2016), these enrichments suggest high sea water participation and a magmatic contribution. Moreover, hydrothermal fluid from the Ilia area shows the highest concentrations of Fe (up to 13,300 μg/L) and As (250 μg/L) compared to any of the other hot springs on NW Euboea island (Kanellopoulos et al., 2017; Table 1). Kanellopoulos et al. (2017, 2018) based on mineralogical and geochemical observations such as (a) the presence of

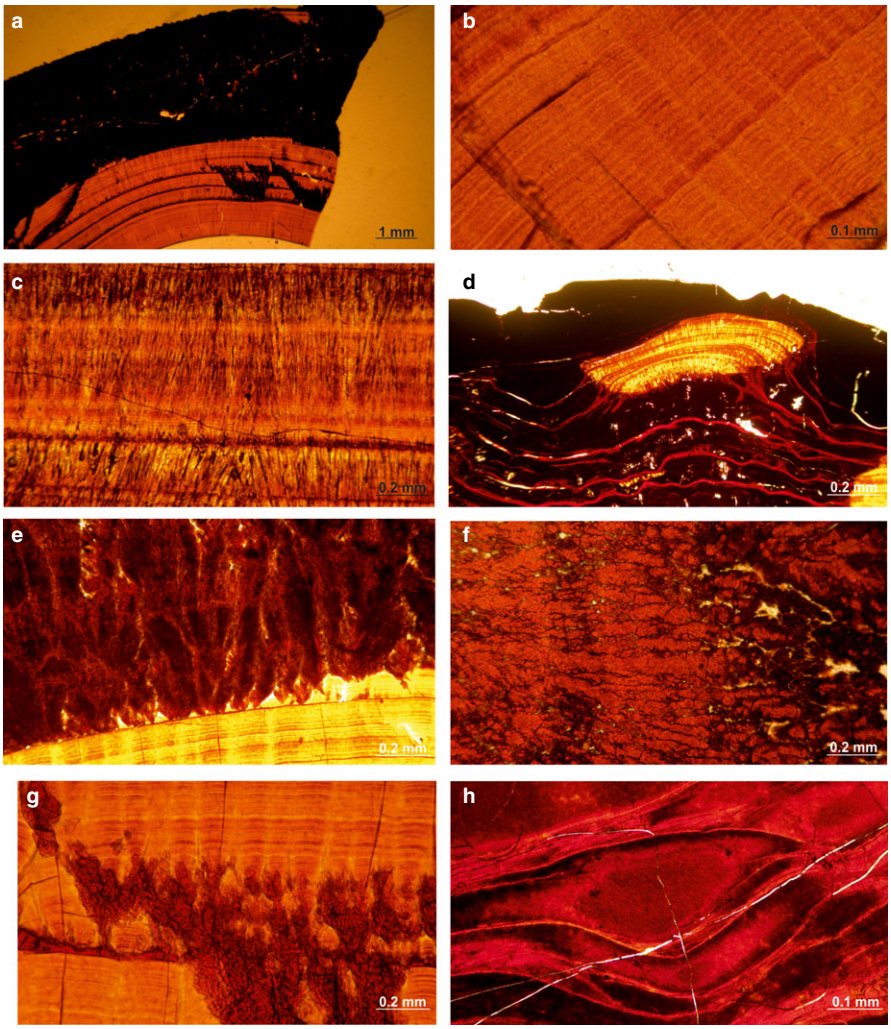


**FIGURE 6** Microscopic features of the travertines, under transmitted-light microscope, with parallel nicols. (a) Well-developed and separated Ca- and Fe-rich components. (b) Close-up of the Ca-rich component composed of numerous growth laminae. (c) Ca-rich laminas separated by laminae of silt-sized micritic aggregates. (d) Ca-rich component develops isolated in a Fe-rich- component. Fe-rich component, even if no crystalline shape could be identified under the optical microscope, it seems that it is also developing in layers/laminas. (e and f) Laterally aligned shrub-like structures creating dendritic fabric extending and branching upwards. At (g) aragonitic laminas have filled up the empty spaces between the Fe-rich shrub-like structures and at the centres of the shrubs could be distinguished filaments often show dark-tinted axes, likely consisting of organic substances, and are encased in ferrihydrite. (h) Fe-rich band consisted of ferrihydrite, even if no crystalline shape could be identified under the optical microscope, it seems that it is also developing in layers/laminas

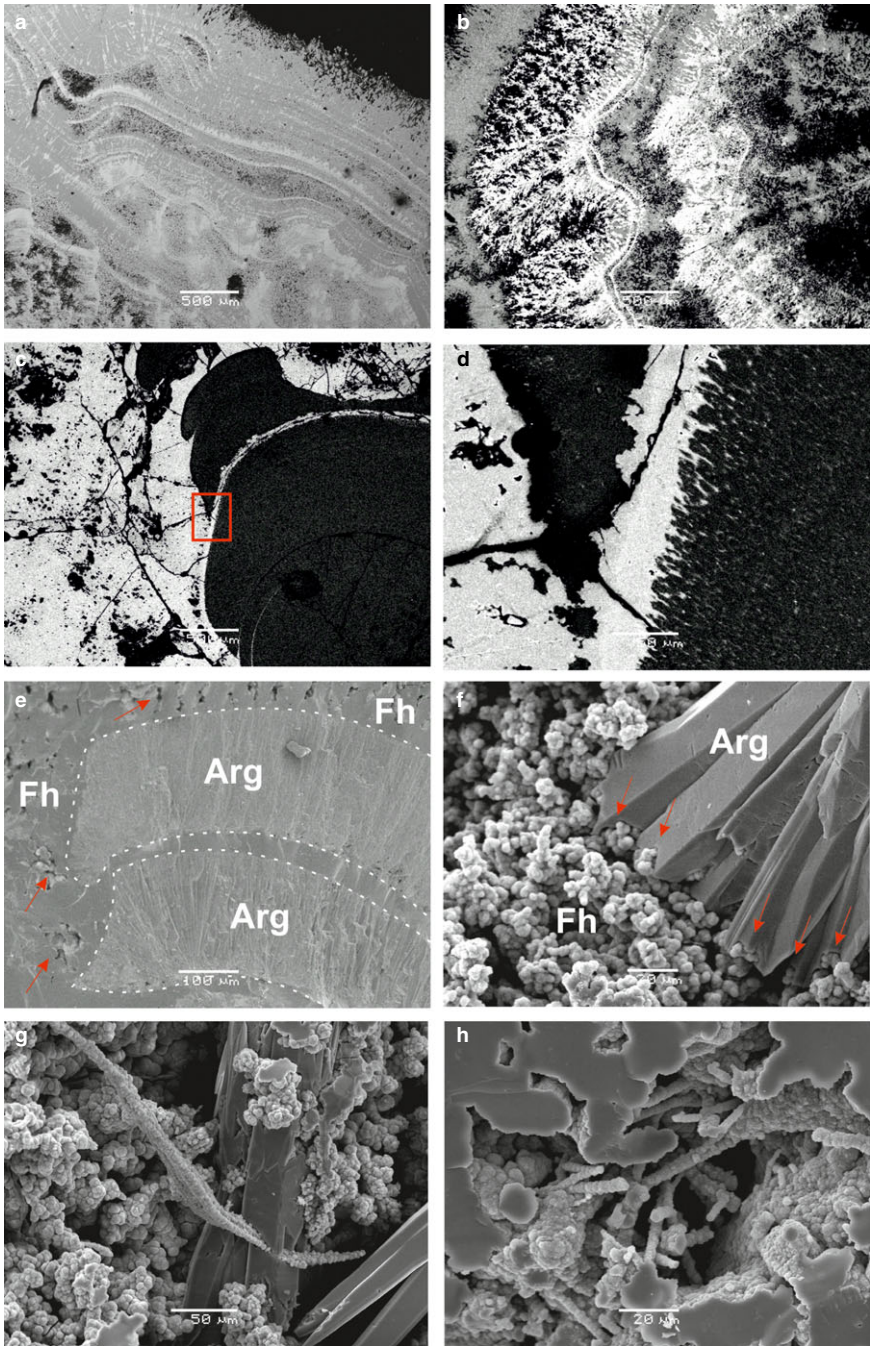


**FIGURE 7** Back-scattered electron images (BSEI: a–d) of laminated travertines from Ilia. Light areas have a higher average atomic weight (Fe-rich) than the dark areas (Ca-rich). And SEM photomicrograph (e–h) of Fe-rich travertines fragments from Ilia (Arg = Aragonite and Fh = Ferrihydrite). (a–b). Numerous growth laminae which have different average atomic weights (Fe-rich and Ca-rich). At image (b) could be seem laterally aligned Fe-rich shrub-like structures extending and branching upwards, creating dendritic fabric and composed by spherical nodules aggregates of about 250 nm. (c) Dense, well-developed and separated laminas of the two phases. Only, the Fe-rich area present some empty spaces. Additionally, (c) is presenting the transition from one lamina to the other. The Fe-rich lamina expands (shrubs) in to the Ca-rich lamina. (d) Close-up of image. (e) Transition from ferrihydrite laminae to aragonite laminae. The aragonite laminae are composed by needle-like crystals (radiating arrays). The crystals are elongated parallel to the c-axis, exhibiting straight extinction and creating dense laminae. The ferrihydrite have been developed filling the empty spaces of the top part of the aragonite crystals, no empty space could be observed. The ferrihydrite laminae are usually also very dense, without any crystallographic habit. Although, in some cases empty spaces between the dendrite aggregations were observed inside the laminas (see arrows). (f) Spherical nodules aggregates of ferrihydrite co-existing with aragonite crystals at the surface of a sample. The aragonite crystals have been developing by following — covering the empty spaces of the ferrihydrite aggregates shrubs (see arrows). (g) Encrusted filaments and EPS with spherical nodules aggregates of ferrihydrite. The aragonite crystals are developing in a way to fill up the empty spaces. (h) Dendritic branches of encrusted filaments with spherical nodules aggregates of ferrihydrite

elements in their native form, such as Fe, Pb, Cu, (b) the presence of native alloys such as Au±Cu-Ag and the enrichment of metalloids such as As, Sb, and (c) the abundance of REE, suggested that the system has a magmatic contribution. As a result, metals and metalloids were mainly derived from magmatic fluids, which after mixing with heated sea waters deposited native elements, sulphide mineralization at depth, and As-Fe-rich travertines in the surface (Kanellopoulos et al., 2017, 2018). The repeated measurements conducted during the last years (including wet and dry seasons, Kanellopoulos et al., 2017) have shown that the physicochemical parameters of the hydrothermal fluid are relatively stable with temperatures varying only from 60.9 to 63.7°C and pH values from 5.9 to 6.45 (Table 1, Figure 2). The results reported here are in line with previously published values.

Terrestrial thermogenic Fe-rich travertines with ferrihydrite have been reported in Shionaha (Takashima & Kano, 2005) and Okuoku-Hachikurou, Japan (Takashima et al., 2008, 2011). Additionally, the presence of ferrihydrite in hydrothermal environments has also commonly been reported in submarine vents (chimneys and hydrothermal sediments) such as the Basiluzzo Islet, Italy (Bortoluzzi et al., 2017), Kolumbo, Greece (Kilias et al., 2013), and Tutum Bay in Papua New Guinea (Pichler & Veizer, 1999). By comparing Ilia's hydrothermal fluid with these occurrences (Table 2), the studied fluids show similar pH values (slightly acidic: 5–6.6). The temperatures of the other known terrestrial ferrihydrite depositing hot springs in Japan are 20–35°C lower, potentially allowing the development of non-thermophilic organisms. Regarding iron, Ilia's hydrothermal fluid shows higher concentrations than the terrestrial hot springs of Japan (Takashima & Kano, 2005; Takashima et al., 2008) and the hydrothermal vent from Tutum Bay (Papua New Guinea; Pichler & Veizer, 2004). However, iron concentrations are lower when compared to the Basiluzzo Islet (Italy; Bortoluzzi et al., 2017) and Kolumbo (Greece; Kilias et al., 2013) submarine vents. Hence, Ilia hot spring shares some similar physicochemical characteristics with the fluids of the above-mentioned areas. Additionally, based on these characteristics Ilia can be ranked among the most iron enriched terrestrial hot springs worldwide, with near neutral pH.

## 5.2 | Iron-rich travertine composition

Based on their strong differences such as their colour and also their facies and chemical composition, it is clear that the Fe-rich and Ca-rich laminae of the travertine are formed under very different conditions. In particular, spatial discrimination of Fe-deposits from Ca-deposits is observed, with a dark colour (representative of iron oxides of the Fe-rich laminae) only present when there is hot water flowing at a relatively high speed. When the flow rate decreases (away from the vent) or where there is no water flow (on the sides of the pipe for example), the orange colour, representative of the Ca-rich component, dominates. These observations strongly suggest that the differential deposits of the Fe-rich and Ca-rich component are controlled by variations in the flow rate of hot water venting from the spring. As a result, it is expected that the laminae are controlled by these changes.

The elements As, Sc, and Y are clearly enriched in the Fe-rich component compared to the Ca-rich component. The strong binding potential of metal oxides towards arsenic could explain this difference in the ferrihydrite-rich component (Smedley & Kinniburgh, 2002). In contrast, the Ca-rich component of the Ilia travertine clearly has higher concentrations of Mn (330 mg/kg) compared to the Fe-rich component. This may be related to the fast oxidation of $Mn^{2+}$ in changing redox conditions, which may have varied between the two different phases. Metals such as Co and Ni follow the same trend. Similarly, the positive Ce anomaly observed in the Ca-rich component could be linked to the sensitivity of Ce to oxidative conditions (Bau & Koschinsky, 2009). Hence, enrichment is observed in elements that become insoluble when oxidized in the Ca-rich component, potentially pointing towards changes in redox conditions during the precipitation of this phase.

## 5.3 | Microbial communities of the travertine deposits of Ilia

Communities of the thermogenic travertines of Ilia vary with changes in water flow, distance to the vent, aerial exposure, and natural redox conditions (Table 1, Figure 9a). The two samples that experienced the highest water flow (ID2 and IP2) are marked by an abundance of thermophilic organism of the *Aquificae* phylum. Sequences of this phylum are uniquely attributed to the family *Hydrogenothermaceae*, which consists of chemolithoautotrophic microaerophilic thermophiles (Takai & Nakagawa, 2014). The other phyla consist mainly of unclassified sequences, except for *Zetaproteobacteria,* which are attributed to the Fe-oxidizers of *Mariprofundaceae* family (Emerson, Fleming, & McBeth, 2010). Interestingly, these Fe-oxidizers are characteristic of marine environments like the Loihi seamount (Emerson & Moyer, 2012), Santorini marine hydrothermal springs (Handley, Boothman, Mills, Pancost, & Lloyd, 2010), or of Basiluzzo Islet in the Aeolian islands (Bortoluzzi et al., 2017). Communities obtained from IP3 and ID3 share similarities allowing a continuum to be drawn between the environments of ID2 and IP2. *Aquificae* and *Zetaproteobacteria* sequences are still present (3.3% and 7.2%). Additionally, species richness is higher, with photosynthetic

**TABLE 3** Whole-rock travertine chemistry of the studied travertines as determined by ICP-MS and ICP-AES analysis and comparison with Fe-rich travertines elsewhere and submarine Fe-rich hydrothermal depositions

| | Terrestrial | | | | | | Submarine | |
|---|---|---|---|---|---|---|---|---|
| | Ilia (Fe-rich part)-Greece | Ilia (Ca-rich part)-Greece | Aedipsos-Greece[1] ($n$ = 23) | Ilia-Greece[1] ($n$ = 3) | N. Caucassus-Russia[2] ($n$ = 56) | Savo Volcano-Solomon Islands[3] ($n$ = 5) | Tutum Bay (submarine hydrothermal aragonite)-Papua New Guinea[4] ($n$ = 4) | Tutum Bay (submarine hydroth. Fe (III). Oxyhydroxide dep.)-Papua New Guinea[6] ($n$ = 7) |
| Ca % | – | – | 3.2–62 | 10.3–21.9 | 0.4–49.3 | 32–37 | 37.2–38.5 | 1.2–5 |
| Fe % | 35.3 | 11 | 0.0049–2.395 | 13.1–28.9 | 0.0114–6.83 | 0.06–2.29 | 0.049–0.126 (up to 29.7)[5] | 31–37.8 |
| Al mg/kg | 1,340 | 1,850 | 6–1,150 | 54–150 | 9–7,475 | – | 530–1,800 | bdl–5,500 |
| As mg/kg | 26,120 | 930 | 66–230 | 4,895–18,300 | – | 0.6–626 | – (up to 33,200)[5] | 4.9–6.2 (%) |
| Ba mg/kg | 117 | 88 | 3–145 | 80–90 | 4–10,890 | 23–167 | bdl–47 | 70–220 |
| Cd mg/kg | 1.1 | bdl | 0.001–0.025 | 0.015–0.018 | – | 0.05–0.36 | bdl–0.4 | – |
| Co µg/kg | 705 | 2,450 | bdl | bdl | bdl–48,200 | 100–2,900 | bdl | bld |
| Cr µg/kg | 16,830 | 26,800 | bdl | bdl | bdl–29,000 | 1,700 | bdl | 16,000–45,000 |
| Cu mg/kg | 6 | 8.4 | 3.6–14.7 | bdl | bdl–58.5 | 0.150–0.780 | bdl–18 | 13–160 |
| K mg/kg | 9,960 | 10,750 | 36–1,090 | 335–510 | bdl–1,270 | bdl–100 | bdl | 996–2,739 |
| Li µg/kg | 6,640 | 8,565 | 140–3,900 | 1,530–1,940 | bdl–88,600 | – | – | – |
| Mg mg/kg | 1,915 | 1,650 | 87–2,990 | 545–690 | bld–41,800 | 900–4,300 | 240–540 | 4,400–7,720 |
| Mn mg/kg | 98 | 330 | 1–1,984 | 74–195 | 5–18,000 | 1,260–7,065 | 77–540 | 542–851 |
| Na mg/kg | 40,480 | 810 | 700–33,100 | 3,280–4,960 | bdl–6,870 | 140–630 | bdl–590 | 3,560–8,080 |
| Ni µg/kg | 7,635 | 15,860 | bdl | bdl | bdl–48,200 | 1,500–4,000 | bdl | 80–550 |
| Pb mg/kg | 4.7 | 2.9 | 0.348–10.6 | 0.72–2.21 | bdl–34.6 | 0.03–1.25 | 7–24. | 14–49 |
| Rb µg/kg | 1,460 | 1,290 | 417–690 | 520–790 | 16–12,400 | | 430–49,000 | 3,800–13,000 |
| S mg/kg | 897 | 2,720 | 230–67,800 | 650–2,740 | 30–6,650 | 1,500–10,500 | bdl | – |
| Sc µg/kg | 73,445 | 4,985 | 130–630 | 2,560–8,870 | – | 100–400 | bdl | bdl |
| Si mg/kg | – | 30,350 | 12–950 | 86–340 | 27–8,140 | – | bdl | 5.7–9.77 (%) |
| Th µg/kg | 720 | 450 | bdl–150 | 9–41 | bdl–3,700 | – | bdl–970 | – |
| U µg/kg | 240 | 290 | 10–91 | 75–200 | bdl–6,500 | bdl–200 | 30–1,100 | 340–920 |
| V µg/kg | 3,970 | – | 140–2,560 | 1,040–2,610 | bdl–28,800 | – | bdl | bdl–80,000 |
| Y µg/kg | 322,790 | 19,700 | 80–7,980 | 71,100–258,900 | 61–86,000 | – | 18,000–90,000 | 8,100–21,000 |
| Zn mg/kg | 63 | 48 | 2.52–25.9 | 16–24.3 | bdl–162 | 0.3–21 | bdl | 24–56 |
| Zr µg/kg | – | – | 29–2,080 | 290–1,070 | bdl–338,000 | – | 700–49,000 | – |
| La µg/kg | 54,760 | 470 | 180–1,100 | 14,300–57,300 | bdl–32,100 | 700–2,700 | – | – |
| Ce µg/kg | 157,070 | 3,920 | 19–1,660 | 27,500–119,300 | 60–78,200 | – | – | – |
| Pr µg/kg | 21,030 | 500 | 2–220 | 3,640–16,900 | 7–8,400 | – | – | – |
| Nd µg/kg | 96,070 | 2,120 | 6–1,110 | 16,700–76,500 | 57–31,000 | – | – | bdl–18,000 |
| Sm µg/kg | 30,520 | 620 | 3–390 | 5,280–24,400 | bdl–7,200 | – | – | – |
| Eu µg/kg | 10,290 | 205 | 1–150 | 1,850–8,300 | bdl–1,700 | – | – | – |
| Gd µg/kg | 49,910 | 1,035 | 6–770 | 8,830–38,400 | 22–8,700 | – | – | – |
| Tb µg/kg | 9,450 | 220 | bdl–140 | 1,750–7,580 | bdl–1,600 | – | – | – |
| Dy µg/kg | 62,920 | 1,565 | 1–950 | 12,700–51,300 | bdl–11,900 | – | – | – |
| Ho µg/kg | 13,330 | 380 | bdl–190 | 2,710–10,800 | bdl–2,800 | – | – | – |
| Er µg/kg | 35,700 | 1,190 | 7–1,140 | 7,570–29,700 | 10–9,800 | – | – | – |
| Tm µg/kg | 4,310 | 160 | bdl–60 | 940–3,760 | bdl–1,700 | – | – | – |
| Yb µg/kg | 24,160 | 875 | 2–300 | 5,230–19,800 | bdl–11,000 | – | – | – |
| Lu µg/kg | 2,960 | 130 | bdl–38 | 650–2,410 | bdl–1,800 | – | – | – |

*Notes*. 1 = Kanellopoulos et al. (2017); 2 = Lavrushin, Kuleshov, and Kikvadze (2006); 3 = Smith (2008); 4 = hydrothermal aragonite, Pichler and Veizer (2004); 5 = sediment cores, Price and Pichler (2005); 6 = hydrothermal Fe III. oxyhydroxide precipitates, Pichler and Veizer (1999); 7 = Kilias et al. (2013); 8 = Hannington et al. (2005); 9 = De Ronde et al. (2002); 10 = Glasby, Iizasa, Hannington, Kubota, and Notsu (2008), bdl = below detection limit.

| Kolumbo-Greece[7] ($n$ = 14) | Brothers (Volcanic arcs)[8] ($n$ = 9) | Lake Taupo massive sulphides (Volcanic arcs)[9] ($n$ = 1) | S. Explorer Ridge (Mid-ocean ridge)[8] ($n$ = 51) | Endeavour Segment Main Field (Mid–ocean ridge)[8] ($n$ = 83) | Average JADE site1 (Back-arc rifts)[10] | Izena cauldron (Back-arc rifts)[8] ($n$ = 40) | Tyrrhenian Sea Panarea (Back-arc basins)[8] ($n$ = 5) | Tyrrhenian Sea Palinuro (Back-arc basins)[8] ($n$ = 15) |
|---|---|---|---|---|---|---|---|---|
| – | – | – | – | – | – | – | – | – |
| 16.6 | 7.4 | 25.3 | 25.2 | 30.1 | 6.2251 | 6.2 | 10.5 | 15.1 |
| – | – | – | – | – | – | – | – | – |
| 3,810 | 2,155 | 588 | 575 | 356 | 17,500 | 17,500 | 505 | 3,400 |
| – | – | – | – | – | – | – | – | – |
| 276 | 105 | – | 200 | 250 | 794 | 820 | 255 | – |
| – | – | – | – | – | – | – | – | – |
| – | – | – | – | – | – | – | – | – |
| 1,640 | 28,000 | 4.2 | 32,000 | 27,000 | 33,000 | 33,000 | 500 | 4,000 |
| – | – | – | – | – | – | – | – | – |
| – | – | – | – | – | – | – | – | – |
| – | – | – | – | – | – | – | – | – |
| – | – | – | – | – | – | – | – | – |
| – | – | – | – | – | – | – | – | – |
| – | – | – | – | – | – | – | – | – |
| 35,000 | 2,000 | 8.2 | 1,000 | 5,000 | 110,800 | 118,000 | 28,000 | 86,000 |
| – | – | – | – | – | – | – | – | – |
| – | – | – | – | – | – | – | – | – |
| – | – | – | – | – | – | – | – | – |
| 14,100 | – | – | 44,409 | 42,539 | 19,634 | 47,214 | 118,735 | – |
| – | – | – | – | – | – | – | – | – |
| – | – | – | – | – | – | – | – | – |
| – | – | – | – | – | – | – | – | – |
| – | – | – | – | – | – | – | – | – |
| 10,200 | 33,000 | 62.5 | 54,000 | 64,000 | 200,200 | 202,000 | 62,000 | 179,000 |
| – | – | – | – | – | – | – | – | – |
| – | – | – | – | – | – | – | – | – |
| – | – | – | – | – | – | – | – | – |
| – | – | – | – | – | – | – | – | – |
| – | – | – | – | – | – | – | – | – |
| – | – | – | – | – | – | – | – | – |
| – | – | – | – | – | – | – | – | – |
| – | – | – | – | – | – | – | – | – |
| – | – | – | – | – | – | – | – | – |
| – | – | – | – | – | – | – | – | – |
| – | – | – | – | – | – | – | – | – |
| – | – | – | – | – | – | – | – | – |
| – | – | – | – | – | – | – | – | – |

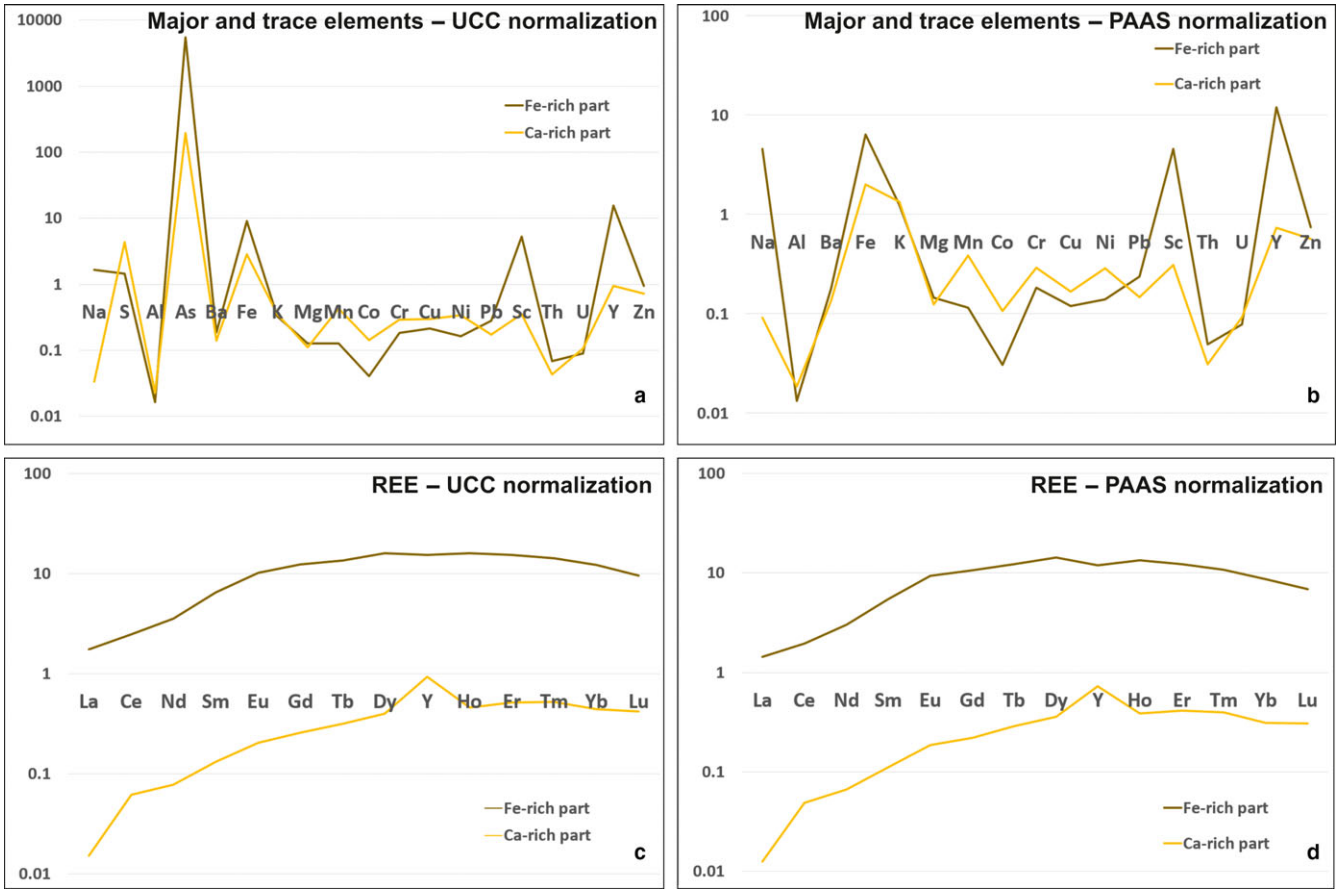


**FIGURE 8** Bulk geochemical analysis of travertine normalized against average Upper Continental Crust (Rudnick & Gao, 2003) and Post-Archaean Australian Shale (PAAS, Taylor & McLennan, 1985). (a and b) Major and trace elements. (c and d) REE

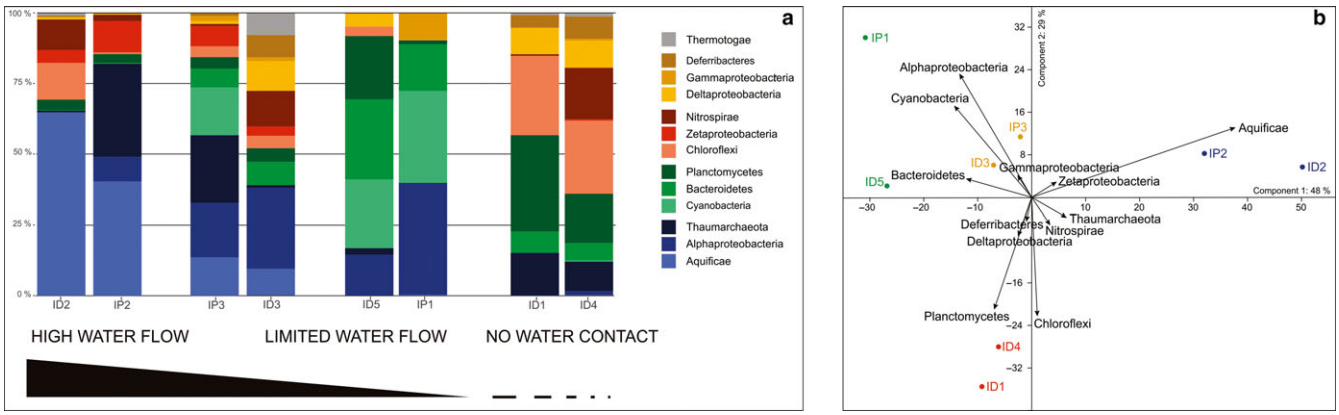


**FIGURE 9** Microbial assemblages (16S rRNA gene sequences) of the Ilia travertine. (a) Composition of the different samples at the phylum level as a function of the water flow exposure. (b) Principal component analysis of the microbial community composition at the phylum level

*Cyanobacteria* in IP3 and a large number of *Bacteroidetes* and *Alphaproteobacteria*. These are widespread clades for which metabolic styles are hard to distinguish at the phylum to family level. However, the coexistence of *Cytophagia, Erythrobacteraceae, Rhodospirillaceae,* and *Rhodobacteraceae* clades suggests a dynamic environment in photic zone (Table 1), with different sources of carbon vis autotrophy and heterotrophy under microaerophilic to aerobic conditions. Sequences obtained from samples ID5 and IP1 show a clear dominance of aerobic metabolisms. No iron-related clade was obtained and visual examination clearly showed photosynthetic activity (green-pigmented travertine interpreted as containing *Cyanobacteria*) for these two samples (Figure 3a,c), as well as in other areas

of the Ilia system where water flow was slow or non-existent (because of daily to monthly flow variations). It is suggested that the high water temperature prevents the development of *Cyanobacteria* in other light exposed systems. This would differentiate this system from the Okuoku-Hachikurou hot spring (Takashima et al., 2011). But as soon as the water flow rate drops or diverges, *Cyanobacteria* take over and dominate the travertine assemblage. Samples ID1 and ID4 show completely different communities (Figure 9b) marked by anaerobic clades. Sequences are attributed to members of the *Planctomycetes*, *Chloroflexi* unclassified or attributed to the *Anaerolinae* class, which consists only of strict anaerobes commonly found in hot spring microbial mats (Hanada & Pierson, 2006), *Defferibacter* and *Deltaproteobacteria*. From the latter class, sequences that could be assigned to an order were either related to *Desulfobacterales*, *Desulfoarculales*, or *Syntrophobacterales*, which all point towards organisms involved in sulphate reduction. *Defferibacter*-associated sequences could only be assigned to the thermophilic anaerobic *Caldithrix* genus that consists of fermenters potentially using nitrate as an electron acceptor (Alauzet & Jumas-Bilak, 2014). Overall, this environment is likely anaerobic and its microbial assemblage relies mainly on the anaerobic degradation of organic carbon, potentially involving sulphate and nitrate reduction.

The 16S rRNA gene analysis revealed the presence of diverse microbial communities, which could be associated with the deposition of ferrihydrite. The compositional variability of the microbial community is indicative of the heterogeneity and dynamic nature of the studied system. Microaerophilic conditions dominate at the vent, where water starts to equilibrate with the ambient oxygen. When the water flow decreases, oxygen content increases and microaerophilic organisms are replaced by aerobic autotrophs and heterotrophs. In buried settings, fermenters and other sulphate reducers degrade the organic matter previously deposited by runoff or past microbial production.

## 5.4 | Biologically induced ferrihydrite precipitation

Ferrihydrite precipitates from oxidation of $Fe^{2+}$ to $Fe^{3+}$ and from rapid hydrolysis of $Fe^{3+}$ in abiotic or biologically aided processes (Jambor & Dutrizac, 1998; Konhauser, 1998). In the case of the Ilia travertine, several lines of evidence suggest that ferrihydrite is mainly precipitated by bacterial activity in microaerophilic conditions. This conclusion is supported by the presence of fabrics showing a close association of ferrihydrite with filamentous textures resembling sheaths formed by *Zetaproteobacteria* (Figures 6g and 7g,h). They are covered with ferrihydrite particles, and are strikingly similar to the structures described in other settings exhibiting the same organisms (Bortoluzzi et al., 2017; Handley et al., 2010; Takashima et al., 2008). In submarine or continental hydrothermal systems, ferrihydrite is interpreted as precipitated by sheathed or stalked iron oxidizers. These sheathed or stalked iron oxidizers are generally encountered in loose sediments without any textural characteristics. Until now, only Takashima et al. (2008) have identified well-preserved erected filaments encased in dendritic structures, in their case in the Shionoha iron-rich travertine deposits although these were preserved in calcite. Encased-filaments from Ilia are visually similar to the Shionoha structures and could possibly be formed by analogous microbe–mineral interactions. In Shionoha spring (Takashima et al., 2011), the central, darker part of the dendritic fabric of the ferrihydrite spherical aggregates has been interpreted as microbially encrusted filaments. *Zetaproteobacteria Mariprofundaceae,* identified in the Ilia travertine 16S rRNA gene library, is known to form these ferrihydrite-covered stalks (Emerson et al., 2007; Handley et al., 2010). In Ilia deposits, they were found in environments of high water flow, which experienced moderate oxygenation that could have allowed their development under microaerophilic conditions (Konhauser, 1998; Takashima et al., 2008). All of the Ilia system data thus suggest microbially aided deposition of ferrihydrite by *Zetaproteobacteria* under microaerophilic conditions.

The second type of ferrihydrite facies, described as dense laminae with limited porosity and no crystalline habit, has been attributed to abiotic precipitation by Kanellopoulos et al. (2017). The findings presented here cannot rule out this hypothesis, and it is possible that ferrihydrite precipitation continues to occur once it has been initiated by the iron-oxidizing bacteria community, potentially evolving from the shrub ferrihydrite facies to porosity-filling by small ferrihydrite spherulites. A geomicrobiological investigation at the lamina scale will be necessary to untangle these processes.

## 5.5 | Proposed model for the precipitation of Banded Iron Travertine (BIT)

The two types of bands (i.e., Fe-rich and Ca-rich) observed in the BIT display different mineralogical, morphological, chemical, and microbiological features, all related to the distinct processes of deposition. Fe-rich bands show relative depletion in elements that are the most sensitive to redox conditions (Mn and Ce), implying more reduced conditions during their precipitation than for the Ca-rich bands. Microbiological analyses of organisms living under these conditions support this kind of redox process, all displaying a significant fraction of iron-oxidizing bacteria from the *Zetaproteobacteria* class. Hence, it is suggested that these microorganisms only develop where microaerophilic

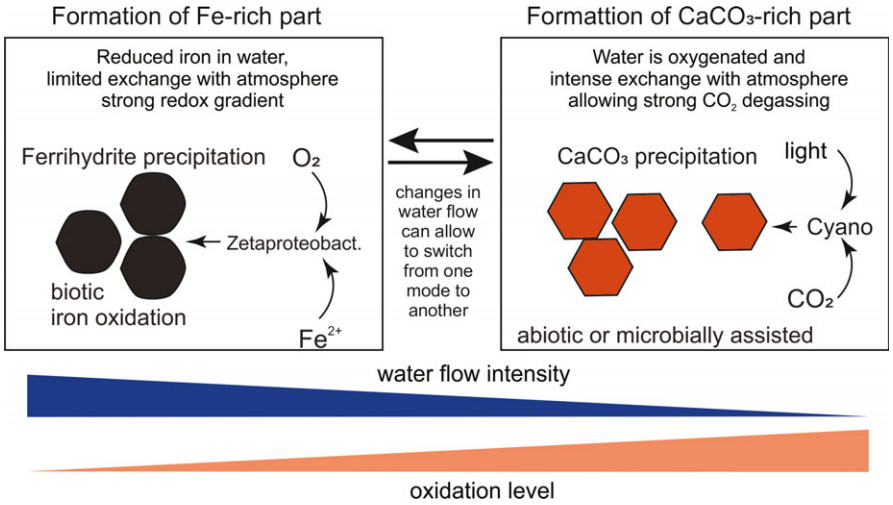


**FIGURE 10** Model for the formation of banded iron travertine of Ilia. Switching from one mode to another might be controlled by variations in the flow of venting water, potentially controlled by volcanic pulses and whatever controls the fluid circulation in the hydrothermal system

conditions prevail, and that they are responsible for most of the primary ferrihydrite precipitation within the iron bands. Due to the significant variations in water flux at the spring, these microaerophilic environments may develop at different levels of the borehole and pipe system. During periods of higher flow, the upcoming reduced spring water will be oxidized further away from the vent, and the site where microaerophilic Fe-oxidizers can develop and precipitate ferrihydrite will move away as well. In conditions of lower flow, fully oxidized conditions may develop in areas that used to be microaerophilic. In such conditions, biologically induced ferrihydrite precipitation would not occur and the $CaCO_3$ precipitation takes over as exposure to the atmosphere allows degassing and travertine formation (Figure 10). Potentially, the development of *Cyanobacteria* in such settings would enhance this $CaCO_3$ formation. Areas of standing water will most likely develop such conditions and evaporative processes accompanying the travertine deposition will allow co-precipitation of halite, as observed in the XRD data (Figure 5).

In the case of the Okuoku-Hachikurou hot spring, a symbiotic relationship between *Cyanobacteria* and Fe-OB was suggested to explain the laminated texture of iron-rich deposits. These laminations were thought to reflect changes in photosynthetic intensity (Takashima et al., 2011). In the Ilia travertines, co-occurrence of *Zetaproteobacteria* and *Cyanobacteria* was not observed, likely because of the more dynamic with higher temperature. The interlayering change of Fe-rich and Ca-rich bands is explained by changes in water flow coming from the vent. It allowed the biologically driven precipitation of the iron bands to alternate with mainly abiotically driven precipitation of the $CaCO_3$ bands in the same location. These changes may be linked to tide cycles as sea water fuels the hydrothermal spring system, or by magmatic pulses. Pulses have been observed on a daily basis in the Euboea hydrothermal system (unpublished results). While cyanobacteria may contribute to the carbonate precipitation in this system, the high precipitation rates suggest that it is unlikely that they play the major role in carbonate precipitation.

## 5.6 | Iron-rich travertines as analogues to BIF

The Ilia travertines are mainly the result of sea water circulation within a hydrothermal system that subsequently leads to the formation of iron-rich deposits, when interacting with oxidative environments, at a geologically fast rate. It leads to deposition of almost pure ferrihydrite laminae alternating with another chemically precipitated facies (here calcium carbonate) that resemble BIF characteristics. In particular, the Ilia travertines have iron enrichment of up to 35 wt%, only comparable with systems like Tutum Bay in Papua New Guinea (Pichler & Veizer, 1999) and the Endeavour Segment Main Field (Hannington, De Ronde, & Petersen, 2005). Even the Ca-rich bands exhibit higher iron concentrations than many active submarine hydrothermal deposits (Table 3), which emphasizes the enormous iron enrichment exhibited by the Ilia travertine and corroborates its resemblance to BIF. As an example, Algoma-type BIF ore grade varies from 15 to 45 wt% (Bekker et al., 2010, 2014; Posth, Konhauser, & Kappler, 2010). Other similarities with the general geological setting of Algoma-type BIFs (Bekker et al., 2010, 2014; Cannon, 1986) are apparent in the Ilia case. The Ilia travertine forms in a back-arc region, after circulation within deeper bedrock including ophiolitic-ultramaphic rocks. Algoma-type BIFs were likely deposited in island arc/back-arc basins (Bekker et al., 2010, 2014; Veizer, 1983) associated with similar (ultra)mafic volcanics (Harnmeijer, 2010; Gourcerol, Thurston, Kontak, Côté-Mantha, & Biczok, 2016).

The entangling of biogenic and abiotic processes is also a salient feature of BIF deposition. Several hypotheses have been suggested concerning the biological influence on BIF deposition (Bekker et al., 2010, 2014): the anoxygenic

phototrophic iron-oxidizing bacteria, which can couple Fe (II) oxidation to the reduction of $CO_2$ (Ehrenreich & Widdel, 1994; Widdel et al., 1993), the cyanobacterial model for BIF formation (Cloud, 1973) or the chemolithoautotrophic iron-oxidizing bacteria living in a neutral pH environment (Holm, 1989). In the case of the BIT of Ilia, the latter model likely explains the process of iron precipitation in the Fe-rich bands. This process, however, relies on the existence of suboxic conditions (incomplete oxygenation of the spring water at the Ilia vent). Similar suboxic conditions could have been encountered during the time of BIF deposition, when oxygen production fuelled by ancestral cyanobacterial activity was only being initiated.

Although, there are some BIF with carbonate bands such as the Cauê Iron Formation in Brazil (Spier, de Oliveira, Sial, & Rios, 2007; Teixeira et al., 2017), BIFs do not typically contain carbonate bands. The mineralogy of BIF generally consists of silica as chert, magnetite, hematite, Fe-rich silicate minerals such as stilpnomelane, minnesotaite, greenalite, and riebeckite, carbonate minerals such as siderite, ankerite, calcite, and dolomite, and in some cases sulphides such as pyrite and pyrrhotite (Bekker et al., 2010, 2014; Koeksoy, Halama, Konhauser, & Kappler, 2016; Gourcerol et al., 2018). The silica considered to have been originated either from the sediment–water interface in colloidal form, by absorption on iron oxyhydroxides from sea water and scavenged with organic matter (Bekker et al., 2010, 2014 Fischer & Knoll, 2009; Grenne & Slack, 2005; Krapez, Barley, & Pickard, 2003), or from replacement of the original sediment, formed beneath the sediment–water interface (Bekker et al., 2014; Krapez et al., 2003). However, all BIFs have undertaken significant modifications either during diagenesis, or during metamorphism. So, their mineralogy is the result of a series of factors, including the bulk composition of the original sediment, the diagenetic conditions, the metamorphic conditions, and the post-depositional fluid flow. Especially, the effects of temperature and pressure have led to mineralogy replacement, recrystallization, and from change to deletion of primary textures (Klein, 2005; Bekker et al., 2014).

The BIT of Ilia interestingly present poorly diagenetically transformed structures and chemical components that could help untangle the primary features of BIFs. For example, the presence of both, ferric and ferrous minerals in BIFs suggests an average oxidation state of $Fe^{2.4+}$ (Klein & Beukes, 1992), which means that 60% of the Fe in BIFs is made up of Fe(II). The BIF mineralogical composition reflects significant post-depositional alteration under diagenetic and metamorphic conditions. The Fe-rich bands, which consist of magnetite and hematite, are most likely to have formed from an initial Fe(III) oxyhydroxide phase such as ferrihydrite (Bekker et al., 2010, 2014; Gauger, Konhauser, & Kappler, 2015; Klein, 2005; Posth, Hegler, Konhauser, & Kappler, 2008). The BIT of Ilia have an almost pure ferrihydrite composition in their Fe-rich bands, which could represent the primary composition of Fe-rich bands in BIFs and therefore may provide a model of BIF depositional characteristics.

Moreover, the BIT of Ilia also procures a model for potential diagenetic processes in precursor bands. The existence of fermenters and sulphate reducers for example, in these Fe-rich reducing environments (Figure 9) attests of organic matter recycling already taking place within sites of actively forming iron bands. The Ilia spring is therefore an interesting and easily accessible laboratory to investigate the initiation of iron mineral precipitation, micro to macrobanding formation and iron and carbon early syn-sedimentary recycling. Overall, the Ilia BIT shares many textural, mineralogical, chemical, and depositional similarities with Algoma-type BIFs. Given its intense precipitation rates, strong iron enrichment and easy access, it is suggested that a thorough investigation of the biotic and abiotic processes involved in this dynamic small-scale system will help in understanding the suite of complex processes that have led to BIFs as we know them today.

## ACKNOWLEDGEMENTS

CK would like to thank the Institute of Geology and Mineral Exploration (I.G.M.E.) – Division of geothermal energy and thermo-metallic waters for the support and collaboration. CT and DA acknowledge the technical and funding support of the University of Geneva as well as the Swiss National Science Foundation (project No. 200021_166308/1).

## CONFLICT OF INTEREST

All authors declare no conflict of interest.

## ORCID

*Christos Kanellopoulos* https://orcid.org/0000-0003-0955-9700
*Camille Thomas* https://orcid.org/0000-0002-7651-2542
*Daniel Ariztegui* https://orcid.org/0000-0001-7775-5127

## REFERENCES

Alauzet, C., & Jumas-Bilak, E. (2014). The Phylum Deferribacteres and the Genus Caldithrix. In E. Rosenberg, E. F. DeLong, S. Lory, E. Stackebrandt, & F. Thompson (Eds.), *The prokaryotes: Other major lineages of bacteria and the archaea* (pp. 595–611). Heidelberg; Berlin, Germany: Springer.

Aronesty, E. (2011). *ea-utils: Command-line tools for processing biological sequencing data*. Durham, NC: Expr Anal.

Athanasoulis, K., Vougioukalakis, G., Xenakis, M., Kavouri, K., Kanellopoulos, C., Christopoulou, M., … Papadatou, M. (2016).

*Diachronic monitoring of hot springs and geothermal fields of Greece*. Athens, Greek: I.G.M.E (in Greek).

Bau, M., & Koschinsky, A. (2009). Oxidative scavenging of cerium on hydrous Fe oxide: Evidence from the distribution of rare earth elements and yttrium between Fe oxides and Mn oxides in hydrogenetic ferromanganese crusts. *Geochemical Journal*, *43*, 37–47. https://doi.org/10.2343/geochemj.1.0005

Bekker, A., Planavsky, N., Krapez, B., Rasmussen, B., Hofmann, A., Slack, J., … Konhauser, K. O. (2014). Iron formations: Their origins and implications for ancient seawater chemistry. In H. Holland, & K. Turekian (Eds.), *Treatise on geochemistry* (Vol. 9, pp. 561–628). Amsterdam, The Netherlands: Elsevier.

Bekker, A., Slack, J. F., Planavsky, N., Krapež, B., Hofmann, A., Konhauser, K. O., & Rouxel, O. J. (2010). Iron formation: The sedimentary product of a complex interplay among mantle, tectonic, oceanic, and biospheric processes. *Economic Geology*, *105*, 467–508. https://doi.org/10.2113/gsecongeo.105.3.467

Bolger, A. M., Lohse, M., & Usadel, B. (2014). Trimmomatic: A flexible trimmer for Illumina sequence data. *Bioinformatics*, *30* (15), 2114–2120. https://doi.org/10.1093/bioinformatics/btu170

Bortoluzzi, G., Romeo, T., La Cono, V., La Spada, G., Smedile, F., Esposito, V., … Andaloro, F. (2017). Ferrous iron- and ammonium-rich diffuse vents support habitat-specific communities in a shallow hydrothermal field off the Basiluzzo Islet (Aeolian Volcanic Archipelago). *Geobiology*, *15*, 664–677. https://doi.org/10.1111/gbi.12237

Cannon, W. F. (1986). Descriptive model of Algoma Fe. In D. P. Cox, & D. A. Singer (Eds.), *Mineral deposit models* (p. 198). U.S. Geological Survey Bulletin 1693.

Chafetz, H. S., & Guidry, S. A. (1999). Bacterial shrubs, crystal shrubs, and ray-crystal shrubs: Bacterial vs. abiotic precipitation. *Sedimentary Geology*, *126*, 57–74. https://doi.org/10.1016/S0037-0738(99)00032-9

Chan, C. S., Fakra, S. C., Emerson, D., Fleming, E. J., & Edwards, K. J. (2011). Lithotrophic iron-oxidizing bacteria produce organic stalks to control mineral growth: Implications for biosignature formation. *ISME Journal*, *5*, 717–727. https://doi.org/10.1038/ismej.2010.173

Chaudhuri, S., Lack, J. G., & Coates, J. D. (2001). Biogenic magnetite formation through anaerobic biooxidation of Fe(II). *Applied and Environment Microbiology*, *67*, 2844–2848. https://doi.org/10.1128/AEM.67.6.2844-2848.2001

Cloud, P. (1973). Paleoecological significance of the banded iron-formation. *Economic Geology*, *68*, 1135–1143. https://doi.org/10.2113/gsecongeo.68.7.1135

D'Alessandro, W., Brusca, L., Kyriakopoulos, K., Bellomo, S., & Calabrese, S. (2014). A geochemical traverse along the "Sperchios Basin e Evoikos Gulf" graben (Central Greece): Origin and evolution of the emitted fluids. *Marine and Petroleum Geology*, *55*, 295–308.

De Ronde, C. E. J., Stoffers, P., Garbe-Schonberg, D., Christensin, B. W., Jones, B., Manconi, R., … Battershill, C. N. (2002). Discovery of active hydrothermal venting in Lake Taupo, New Zealand. *Journal of Volcanology and Geothermal Research*, *115*, 257–275. https://doi.org/10.1016/S0377-0273(01)00332-8

Dotsika, E. (2015). H-O-C-S isotope and geochemical assessment of the geothermal area of Central Greece. *Journal of Geochemical Exploration*, *150*, 1–15. https://doi.org/10.1016/j.gexplo.2014.11.008

Edgar, R. C., Haas, B. J., Clemente, J. C., Quince, C., & Knight, R. (2011). UCHIME improves sensitivity and speed of chimera detection. *Bioinformatics*, *27*, 2194–2200. https://doi.org/10.1093/bioinformatics/btr381

Ehrenreich, A., & Widdel, F. (1994). Anaerobic oxidation of ferrous iron by purple bacteria, a new type of phototrophic metabolism. *Applied and Environment Microbiology*, *60*, 4517–4526.

Emerson, D., Fleming, E. J., & McBeth, J. M. (2010). Iron-oxidizing bacteria: An environmental and genomic perspective. *Annual Review of Microbiology*, *64*, 561–583. https://doi.org/10.1146/annurev.micro.112408.134208

Emerson, D., & Moyer, C. L. (2012). Neutrophilic Fe-Oxidizing Bacteria are abundant at the Loihi Seamount Hydrothermal Vents and Play a Major Role in Fe Oxide Deposition. *Applied and Environment Microbiology*, *68*, 3085–3093.

Emerson, D., Rentz, J. A., Lilburn, T. G., Davis, R. E., Aldrich, H., Chan, C., & Moyer, C. L. (2007). A novel lineage of proteobacteria involved in formation of marine Fe-oxidizing microbial mat communities. *PLoS ONE*, *2*, e667.

Fischer, W. W., & Knoll, A. H. (2009). An iron shuttle for deepwater silica in Late Archean and Early Paleoproterozoic iron formation. *Geological Society of America Bulletin*, *121*, 222–235.

Gauger, T., Konhauser, K., & Kappler, A. (2015). Protection of phototrophic iron(II)-oxidizing bacteria from UV irradiation by biogenic iron(III) minerals: Implications for early Archean banded iron formation. *Geology*, *43*, 1067–1070. https://doi.org/10.1130/G37095.1

Gkioni-Stavropoulou, G. (1998). *Hydrogeological study of hot and mineral springs of Euboean – Maliac gulf*. Athens, Greek: IGME (in Greek).

Glasby, G. P., Iizasa, K., Hannington, M., Kubota, H., & Notsu, K. (2008). Mineralogy and composition of Kuroko deposits from northeastern Honshu and their possible modern analogues from the Izu-Ogasawara (Bonin) Arc south of Japan: Implications for mode of formation. *Ore Geology Reviews*, *34*, 247–560.

Gourcerol, B., Kontak, D. J., Thurston, P. C., & Petrus, J. A. (2018). Results of LA-ICP-MS sulfide mapping from Algoma-type BIF gold systems with implications for the nature of mineralizing fluids, metal sources, and deposit models. *Mineralium Deposita*, *53* (6), 871–894. https://doi.org/10.1007/s00126-017-0788-7

Gourcerol, B., Thurston, P. C., Kontak, D. J., Côté-Mantha, O., & Biczok, J. (2016). Depositional setting of Algoma-type banded iron formation. *Precambrian Research*, *281*, 47–79. https://doi.org/10.1016/j.precamres.2016.04.019

Grenne, T., & Slack, J. F. (2005). Geochemistry of jasper beds from the Ordovician Løkken ophiolite, Norway: Origin of proximal and distal siliceous exhalites. *Economic Geology*, *100*, 1511–1527. https://doi.org/10.2113/gsecongeo.100.8.1511

Hammer, Ø., Harper, D., & Ryan, P. (2001). PAST: Paleontological statistics software package for education and data analysis. *Palaeontologia Electronica*, *4*, 9.

Hanada, S., & Pierson, B. K. (2006). The family Chloroflexaceae. In M. Dworkin, S. Falkow, E. Rosenberg, K.-H. Schleifer, & E. Stackebrandt (Eds.), *The prokaryotes: Volume 7: Proteobacteria: Delta, epsilon subclass* (pp. 815–842). New York, NY: Springer, New York.

Handley, K. M., Boothman, C., Mills, R. A., Pancost, R. D., & Lloyd, J. R. (2010). Functional diversity of bacteria in a ferruginous hydrothermal sediment. *ISME Journal*, *4*, 1193–1205. https://doi.org/10.1038/ismej.2010.38

Hannington, M. D., De Ronde, C. E. J., & Petersen, S. (2005). Sea-floor tectonics and submarine hydrothermal systems. *Society of Economic Geologists*, *100*, 111–141.

Harnmeijer, J. (2010). *Squeezing Blood from A Stone: Inferences into the life and depositional environments of the early Archaean*. Ph.D. thesis, University of Washington, Washington, DC.

Hatzis, M., Kavouridis, T., Bakalopoulos, P., & Xenakis, M. (2008). *Investigation and determination of Northern Euboea geothermal fields*. Athens, Greek: IGME (in Greek).

Holm, N. G. (1987). Possible biological origin of banded iron-formations from hydrothermal solutions. *Origins of Life*, *17*, 229–250.

Holm, N. G. (1989). The $^{13}C/^{12}C$ ratios of siderite and organic matter of a modern metalliferous hydrothermal sediment and their implications for banded iron formations. *Chemical Geology*, *77*, 41–45. https://doi.org/10.1016/0009-2541(89)90013-2

Jambor, J. L., & Dutrizac, J. E. (1998). Occurrence and constitution of natural and synthetic ferrihydrite, a widespread iron oxyhydroxide. *Chemical Reviews*, *98*, 2549–2585. https://doi.org/10.1021/cr970105t

Kanellopoulos, C. (2011). *Geochemical research on the distribution of metallic and other elements in the cold and thermal groundwater, soils and plants in Fthiotida Prefecture and N. Euboea. Environmental impact*. PhD Thesis, National and Kapodistrian University of Athens, Athens, Greece (in Greek with English abstract).

Kanellopoulos, C. (2012). Distribution, lithotypes and mineralogical study of newly formed thermogenic travertines in Northern Euboea and Eastern Central Greece. *Open Geosciences (Former Central European Journal of Geosciences)*, *4*(4), 545–560. https://doi.org/10.2478/s13533-012-0105-z

Kanellopoulos, C. (2013). Various morphological types of thermogenic travertines in northern Euboea and Eastern Central Greece. *Bulletin of the Geological Society of Greece*, *XLVII/4*, 1929–1938. https://doi.org/10.12681/bgsg.10958

Kanellopoulos, C., Mitropoulos, P., Valsami-Jones, E., & Voudouris, P. (2017). A new terrestrial active mineralizing hydrothermal system associated with ore-bearing travertines in Greece (northern Euboea Island and Sperchios area). *Journal of Geochemical Exploration*, *179*, 9–24. https://doi.org/10.1016/j.gexplo.2017.05.003

Kanellopoulos, C., Valsami-Jones, E., Voudouris, P., Stouraiti, C., Moritz, R., Mavrogonatos, C., & Mitropoulos, P. (2018). A new occurrence of terrestrial native iron in the earth's surface: The Ilia Thermogenic Travertine Case, Northwestern Euboea, Greece. *Geosciences*, *8*, 297. https://doi.org/10.3390/geosciences8080287

Kappler, A., & Newman, D. K. (2004). Formation of Fe(III)-minerals by Fe(II)- oxidizing photoautotrophic bacteria. *Geochimica et Cosmochimica Acta*, *68*, 1217–1226. https://doi.org/10.1016/j.gca.2003.09.006

Karastathis, V. K., Papoulia, J., Di Fiore, B., Makris, J., Tsambas, A., Stampolidis, A., & Papadopoulos, G. A. (2011). Deep structure investigations of the geothermal field of the North Euboean Gulf, Greece, using 3-D local earthquake tomography and Curie Point Depth analysis. *Journal of Volcanology and Geothermal Research*, *206*, 106–120. https://doi.org/10.1016/j.jvolgeores.2011.06.008

Kasama, T., & Murakami, T. (2001). The effect of microorganisms on Fe precipitation rate at neutral pH. *Chemical Geology*, *180*, 117–128. https://doi.org/10.1016/S0009-2541(01)00309-6

Kilias, S. P., Nomikou, P., Papanikolaou, D., Polymenakou, P. N., Godelitsas, A., Argyraki, A., … Scoullos, M. (2013). New insights into hydrothermal vent processes in the unique shallow-submarine arc-volcano, Kolumbo (Santorini), Greece. *Natural Scientific Reports*, *3*, 2421. https://doi.org/10.1038/srep02421

Klein, C. (2005). Some Precambrian banded iron-formations (BIFs) from around the world: Their age, geologic setting, mineralogy, metamorphism, geochemistry, and origin. *American Mineralogist*, *90*, 1473–1499. https://doi.org/10.2138/am.2005.1871

Klein, C., & Beukes, N. J. (1992). Time distribution, stratigraphy, and sedimentologic setting, and geochemistry of Precambrian iron-formations. In J. W. Schopf, & C. Klein (Eds.), *The proterozoic biosphere: A multidisciplinary study* (pp. 139–146). Cambridge, UK: University of Cambridge. https://doi.org/10.1017/CBO9780511601064

Koeksoy, E., Halama, M., Konhauser, K. O., & Kappler, A. (2016). Using modern ferruginous habitats to interpret Precambrian banded iron formation deposition. *International Journal of Astrobiology*, *15*(3), 205–217. https://doi.org/10.1017/S1473550415000373

Konhauser, K. O. (1998). Diversity of bacterial iron mineralization. *Earth-Science Review*, *43*, 91–121. https://doi.org/10.1016/S0012-8252(97)00036-6

Konhauser, K. O., Hamade, T., Raiswell, R., Morris, R. C., Ferris, F. G., Southam, G., & Canfield, D. E. (2002). Could bacteria have formed the Precambrian banded iron formation? *Geology*, *30*, 1079–1082. https://doi.org/10.1130/0091-7613(2002)030<1079:CBHFTP>2.0.CO;2

Kozich, J. J., Westcott, S. L., Baxter, N. T., Highlander, S. K., & Schloss, P. D. (2013). Development of a dual-index sequencing strategy and curation pipeline for analyzing amplicon sequence data on the miseq illumina sequencing platform. *Applied and Environment Microbiology*, *79*(17), 5112–5120. https://doi.org/10.1128/AEM.01043-13

Krapez, B., Barley, M. E., & Pickard, A. L. (2003). Hydrothermal and resedimented origins of the precursor sediments to banded iron formations: Sedimentological evidence from the early Palaeoproterozoic Brockman Supersequence of Western Australia. *Sedimentology*, *50*, 979–1011. https://doi.org/10.1046/j.1365-3091.2003.00594.x

Lavrushin, V., Kuleshov, V., & Kikvadze, O. (2006). Travertines of the Northern Caucasus. *Lithology and Mineral Resources*, *41*(2), 137–164. https://doi.org/10.1134/S0024490206020040

Pe-Piper, G., & Piper, D. (2002). *The igneous rocks of Greece, the anatomy of an orogeny*. Berlin, Germany: Ge-bruder Borntraeger.

Pichler, T., & Veizer, J. (1999). The chemical composition of shallow-water hydrothermal fluids in Tutum Bay, Ambitle Island, Papua New Guinea and their effect on ambient seawater. *Marine Chemistry*, *64*, 229–252. https://doi.org/10.1016/S0304-4203(98)00076-0

Pichler, T., & Veizer, J. (2004). The precipitation of aragonite from shallow-water hydrothermal fluids in a coral reef, Tutum Bay, Ambitle Island, Papua New Guinea. *Chemical Geology*, *207*, 31–45. https://doi.org/10.1016/j.chemgeo.2004.02.002

Posth, N. R., Hegler, F., Konhauser, K. O., & Kappler, A. (2008). Alternating Si and Fe deposition caused by temperature fluctuations in Precambrian oceans. *Nature Geoscience*, *1*(10), 703–708. https://doi.org/10.1038/ngeo306

Posth, N. R., Konhauser, K. O., & Kappler, A. (2010). Banded iron formations. In V. Thiel, & J. Reitner (Eds.), *Encyclopedia of geobiology*. Heidelberg, Germany: Springer.

Posth, N. R., Konhauser, K. O., & Kappler, A. (2013). Microbiological processes in banded iron formation deposition. *Sedimentology*, *60*, 1733–1754. https://doi.org/10.1111/sed.12051

Price, R. E., & Pichler, T. (2005). Distribution, speciation and bioavailability of arsenic in a shallow-water submarine hydrothermal system, Tutum Bay, Ambitle Island. *Chemical Geology*, *224*, 122–135. https://doi.org/10.1016/j.chemgeo.2005.07.017

Quast, C., Pruesse, E., Yilmaz, P., Gerken, J., Schweer, T., Yarza, P., … Glöckner, F. O. (2013). The SILVA ribosomal RNA gene database project: Improved data processing and web-based tools. *Nucleic Acids Research*, *41*, D590–D596.

Ramsey, M. H., Thompson, M., & Banerjee, E. K. (1987). A realistic assessment of analytical data quality from inductively coupled plasma atomic emission spectrometry. *Analytical Proceedings*, *24*, 260–265. https://doi.org/10.1039/ap9872400260

Ring, U., Glodny, J., Will, T., & Thomson, S. (2010). The Hellenic Subduction System: High-Pressure Metamorphism, Exhumation, Normal Faulting, and Large-Scale Extension. *Annual Review of Earth and Planetary Sciences*, *38*, 45–76. https://doi.org/10.1146/annurev.earth.050708.170910

Rudnick, R. L., & Gao, S. (2003). Composition of the continental crust. In R. L. Rudnick (Ed.), *The crust* (Vol. 3, pp. 1–64). Amsterdam, The Netherlands: Elsevier.

Schloss, P. D., Westcott, S. L., Ryabin, T., Hall, J. R., Hartmann, M., Hollister, E. B., … Weber, C. F. (2009). Introducing mothur: Open-source, platform-independent, community-supported software for describing and comparing microbial communities. *Applied and Environment Microbiology*, *75*, 7537–7541. https://doi.org/10.1128/AEM.01541-09

Shimizu, A., Sumino, H., Nagao, K., Notsu, K., & Mitropoulos, P. (2005). Variation in noble gas isotopic composition of gas samples from the Aegean arc, Greece. *Journal of Volcanology and Geothermal Research*, *140*(4), 321–339. https://doi.org/10.1016/j.jvolgeores.2004.08.016

Smedley, P. L., & Kinniburgh, D. G. (2002). A review of the source, behaviour and distribution of arsenic in natural waters. *Applied Geochemistry*, *17*, 517–568. https://doi.org/10.1016/S0883-2927(02)00018-5

Smith, D. (2008). *From slab to sinter: The magmatic-hydrothermal system of Savo volcano, Solomon Islands*. PhD Thesis, University of Leicester, Leicester, UK.

Spier, C. A., de Oliveira, S. M. B., Sial, A. N., & Rios, F. J. (2007). Geochemistry and genesis of the banded iron formations of the Caue Formation, Quadrilatero Ferrifero, Minas Gerais, Brazil. *Precambrian Research*, *152*, 170–206. https://doi.org/10.1016/j.precamres.2006.10.003

Takai, K., & Nakagawa, S. (2014). *The Prokaryotes*. Berlin, Heidelberg: Springer.

Takashima, C., & Kano, A. (2005). Depositional processes of travertine developed at Shionoha hot spring, Nara Prefecture, Japan. *The Journal of the Geological Society of Japan*, *111*, 751–764. https://doi.org/10.5575/geosoc.111.751

Takashima, C., Kano, A., Naganuma, T., & Tazaki, K. (2008). Laminated iron texture by iron-oxidizing bacteria in a calcite travertine. *Geomicrobiology Journal*, *25*(3–4), 193–202. https://doi.org/10.1080/01490450802081887

Takashima, C., Okumura, T., Nishida, S., Koike, H., & Kano, A. (2011). Bacterial symbiosis forming laminated iron-rich deposits in Okuoku-hachikurou hot spring, Akita Prefecture, Japan. *Island Arc Journal*, *20*, 294–304. https://doi.org/10.1111/j.1440-1738.2011.00768.x

Taylor, S. R., & McLennan, S. H. (1985). *The continental crust: Its composition and evolution* Oxford, UK: Blackwell, 312 pp.

Teixeira, N. L., Caxito, F. A., Rosière, C. A., Pecoits, E., Vieira, L., Frei, R., … Poitrasson, F. (2017). Trace elements and isotope geochemistry (C, O, Fe, Cr) of the Cauê iron formation, Quadrilátero Ferrífero, Brazil: Evidence for widespread microbial dissimilatory iron reduction at the Archean/Paleoproterozoic transition. *Precambrian Research*, *298*, 39–55. https://doi.org/10.1016/j.precamres.2017.05.009

Vakalopoulos, P., Xenakis, M., Vougioukalakis, G., Kanellopoulos, C., Christopoulou, M., & Statha, F. (2016). *Medium – High enthalpy geothermal exploration in Edipsos area*. Athens, Greek: IGME (in Greek).

Veizer, J. (1983). Chemical diagenesis of carbonates: Theory and application of trace element technique. In M. A. Arthur, T. F. Anderson, I. R. Kaplan, J. Veizer, & L. S. Land (Eds.), *Stable Isotopes in Sedimentary Geology* (Vol. 10, pp. III-1–III-100). Society of Economic Paleontologists and Mineralogists Short Course Notes. https://doi.org/10.2110/scn.83.10

Vött, A. (2007). Relative sea level changes and regional tectonic evolution of seven coastal areas in NW Greece since the mid-Holocene. *Quaternary Science Reviews*, *26*(7–8), 894–919. https://doi.org/10.1016/j.quascirev.2007.01.004

Wang, Q., Garrity, G. M., Tiedje, J. M., & Cole, J. R. (2007). Naïve Bayesian classifier for rapid assignment of rRNA sequences into the new bacterial taxonomy. *Applied and Environment Microbiology*, *73*, 5261–5267. https://doi.org/10.1128/AEM.00062-07

Wang, Y., & Qian, P. Y. (2009). Conservative fragments in bacterial 16S rRNA genes and primer design for 16S ribosomal DNA amplicons in metagenomic studies. *PLoS ONE*, *4*(10), e7401. https://doi.org/10.1371/journal.pone.0007401

Widdel, F., Schnell, S., Heising, S., Ehrenreich, A., Assmus, B., & Schink, B. (1993). Ferrous iron oxidation by anoxygenic phototrophic bacteria. *Nature*, *362*, 834–836. https://doi.org/10.1038/362834a0

## SUPPORTING INFORMATION

Additional supporting information may be found online in the Supporting Information section at the end of the article.

**How to cite this article:** Kanellopoulos C, Thomas C, Xirokostas N, Ariztegui D. Banded Iron Travertines at the Ilia Hot Spring (Greece): An interplay of biotic and abiotic factors leading to a modern Banded Iron Formation analogue?. *Depositional Rec*. 2018;00:1–23. https://doi.org/10.1002/dep2.55

# Graphical Abstract

The contents of this page will be used as part of the graphical abstract of html only.
It will not be published as part of main article.

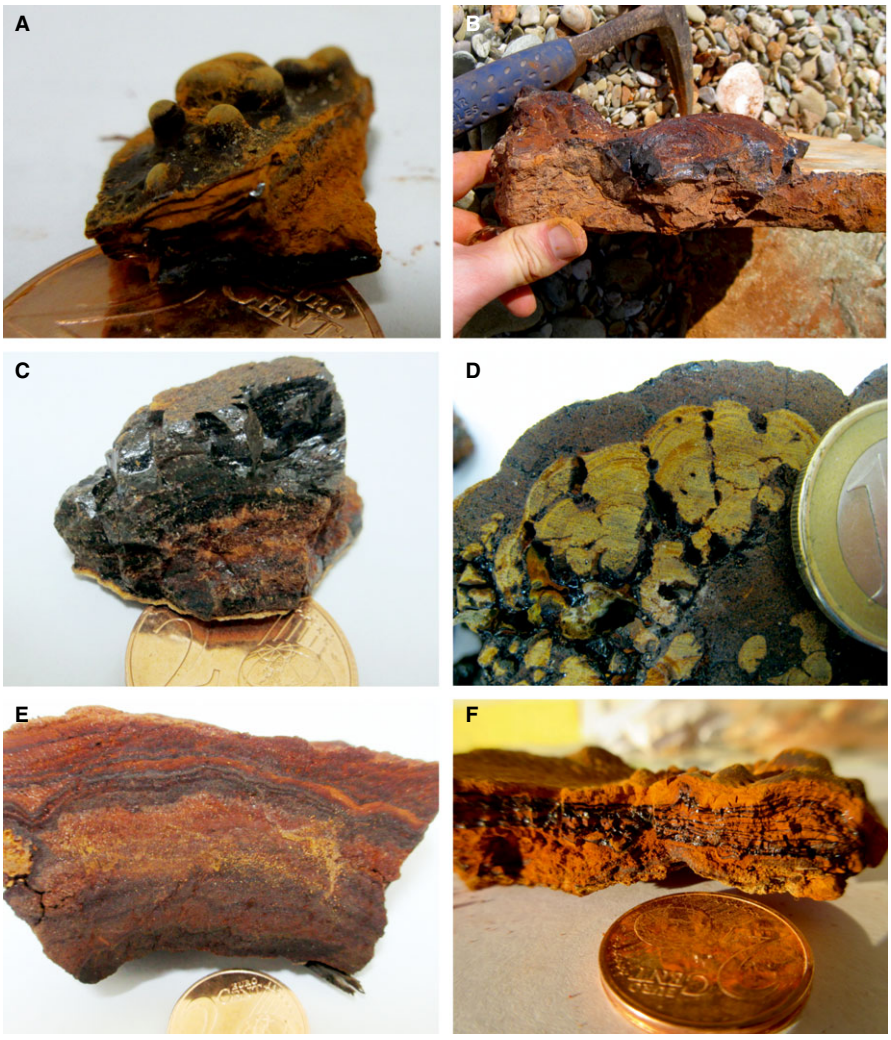


“Banded iron formations” (BIFs) represent archives of the Earth's primitive biogeochemical conditions. The complex associations of abiotic and biotic processes that have likely led to their formation are not fully resolved yet. Here, we present a hydrothermal system from the Greek Island of Euboea, which precipitates iron-rich travertine at an ore-grade concentration (up to 35.3 wt% Fe). These chemical sediments consist of micrometric to centimetric bands of iron oxyhydroxides (ferrihydrite) alternating with calcium carbonate (aragonite)-dominated layers similar to BIFs.